Elucidation of the biosynthesis of the methane catalyst coenzyme F_{430}

Simon J. Moore[1], Sven T. Sowa[2], Christopher Schuchardt[2], Evelyne Deery[1], Andrew D. Lawrence[1], José Vazquez Ramos[2], Susan Billig[4], Claudia Birkemeyer[4], Peter T. Chivers[5], Mark J. Howard[1], Stephen E. J. Rigby[3], Gunhild Layer[2]* and Martin J. Warren[1]*

[1]School of Biosciences, University of Kent, Giles Lane, Canterbury, Kent CT2 7NJ, UK

[2]Institute of Biochemistry, Leipzig University, 04103 Leipzig, Germany

[3]Manchester Institute of Biotechnology, School of Chemistry, University of Manchester, 131 Princess Street, Manchester M1 7DN, UK

[4]Institute of Analytical Chemistry, Leipzig University, 04103 Leipzig, Germany

[5]Department of Chemistry, School of Biological and Biomedical Sciences, Durham University, Durham DH1 3LE, UK

*Correspondence: m.j.warren@kent.ac.uk; gunhild.layer@uni-leipzig.de

Running title: *Coenzyme F_{430} biosynthesis*

Summary

Methane biogenesis in methanogens is mediated by methyl-coenzyme M reductase, an enzyme that is also responsible for the utilisation of methane through anaerobic methane oxidation. The enzyme employs an ancillary factor called coenzyme F_{430}, a nickel-containing modified tetrapyrrole that promotes catalysis through a novel methyl radical/Ni(II)-thiolate intermediate. However, the biosynthesis of coenzyme F_{430} from the common primogenitor uroporphyrinoge III, incorporating 11 steric centres into the macrocycle, has remained poorly understood although the pathway must involve chelation, amidation, macrocyclic ring reduction, lactamisation and carbocyclic ring formation. We have now identified the proteins that catalyse coenzyme F_{430} biosynthesis from sirohydrochlorin, termed CfbA-E, and shown their activity. The research completes our understanding of how nature is able to construct its repertoire of tetrapyrrole-based life pigments, permitting the development of recombinant systems to utilise these metalloprosthetic groups more widely.

Introduction

Coenzyme F_{430} is a modified tetrapyrrole that is required by methyl-coenzyme M reductase (MCR), the terminal enzyme in the process of methanogenesis (Figure 1)[1,2]. This cofactor is responsible for the generation of about a billion tons of methane gas per annum, roughly one third of which escapes into the atmosphere where it is photochemically converted into CO_2[2], thus contributing to the greenhouse effect and global warming. More recently, MCR has also been implicated in the process of reverse methanogenesis (anaerobic methane oxidation)[3-6], which is mediated by bacterial/archaeal mats on the ocean floor. MCR is an enzyme ensemble consisting of a dimer of heterotrimers ($\alpha_2\beta_2\gamma_2$), catalyzing the reversible reduction of methyl-coenzyme M (CH_3-S-CoM) and coenzyme B (HS-CoB) into the heterodisulfide CoM-S-S-CoB and methane[7]. Central to the mechanism of this powerful redox catalyst[8,9] is the nickel porphinoid, coenzyme F_{430} (-650 mV $Ni^{+}/^{2+}$ redox couple). Despite the indispensable role played by coenzyme F_{430} in the process of methanogenesis and carbon cycling, the assembly of this unique cofactor had not been determined[10].

As a modified tetrapyrrole the synthesis of coenzyme F_{430} is based upon the macrocyclic template of uroporphyrinogen III[11,12], from which all hemes, chlorophylls, sirohemes, corrins, bilins and heme d_1 are derived. However, coenzyme F_{430} differs from these other modified tetrapyrroles in the nature of the centrally chelated metal ion and in the oxidation state of the macrocycle, a tetrahydroporphyrinogen, the most reduced member of the family[13]. As well as the four pyrrole-derived rings found in all modified tetrapyrroles (labelled A-D; Figure 1), coenzyme F_{430} also contains two extra rings (E and F; Figure 1). Ring E is a lactam derived

from the amidated acetic acid side chain attached to ring B, whilst the keto-containing ring F originates from the propionic acid side chain on ring D. Radiolabelling experiments indicated that the biosynthesis of coenzyme F_{430} proceeds via sirohydrochlorin, the metal-free precursor of siroheme[14]. Moreover, under depleted nickel growth conditions, *Methanothermobacter marburgensis* was found to accumulate a 15,17^3-*seco* intermediate (*seco*-F_{430}) missing ring F[15]. This intermediate could be converted into coenzyme F_{430} by cell-free extracts in the presence of ATP[15] indicating that this *seco*-F_{430} may represent the penultimate intermediate in the biosynthetic pathway.

Potential gene clusters

With the knowledge that the biosynthesis of coenzyme F_{430} has to involve metal ion chelation, side chain amidation and macrocyclic ring reduction, we sought the clustering of corresponding potential genes for coenzyme F_{430} biosynthesis (given the acronym *cfb*) within the genomes of a range of methanogens. Strikingly, this approach allowed us to identify such a grouping in a number of methanogens, including *Methanosarcina barkeri, Methanomassiliicoccus intestinalis* and *Methanocella conradii,* as shown in Figure 1. These clusters all contain genes for a small type II chelatase[16] (CfbA), followed by a MurF-like ligase[17] (CfbB) and orthologues of the NifD and NifH components of nitrogenase (CfbC and CfbD, respectively). Interestingly, the latter are also orthologues of BchN and BchL of the tetrapyrrole-reducing protochlorophyllide reductase (DPOR)[18], which are involved in bacteriochlorophyll synthesis. Finally, the last gene of the cluster encodes an amidase (CfbE) that is similar to the CobB/CbiA *a*,*c*-diamide synthetase enzymes found in cobalamin biosynthesis[19]. Significantly, *M. intestinalis,* further, contains the genes for the transformation of glutamic acid into precorrin-2, the direct precursor of sirohydrochlorin, within the same gene cluster. The *cfb* genes from *M. barkeri* were amplified and cloned to allow for the characterisation of the encoded products (Extended Data Table 1).

Nickel chelatase CfbA

We had previously shown that CfbA (Mbar_A0344) is able to act as a cobaltochelatase and named it CbiX^S. In this current study, using a higher concentration of Ni^{2+} in the assays, 50 µM rather than 20 µM, the conversion of sirohydrochlorin to Ni^{2+}-sirohydrochlorin by CfbA/CbiX^S could be followed by UV/Vis absorption spectroscopy (Extended Data Figure 1), demonstrating that CfbA/CbiX^S is able to catalyse the insertion of nickel as well as cobalt into sirohydrochlorin *in vitro*. The specific activity of CfbA/CbiX^S for Ni^{2+} insertion *in vitro* was determined as 3.4±0.5 nmol min^{-1} mg^{-1}, which is considerably lower than that observed for Co^{2+} insertion (122 nmol min^{-1} mg^{-1})[16]. The assays were performed with reagents that were originally devised for cobalt insertion and therefore optimization is required through the use

of different buffers and pH values to determine conditions that may allow for enhanced Ni^{2+} insertion. Hence, the *in vivo* activity of the chelatase enzyme might be much faster than that observed *in vitro*.

To this end the activity of CfbA as a nickel-chelatase was also probed *in vivo*. Under aerobic conditions *E. coli* does not import nickel, although anaerobically a high affinity multicomponent system, *nikA-E*, is activated[20-22]. We attempted to produce Ni^{2+}-sirohydrochlorin in *E. coli* by linking the expression of the genes for the production of precorrin-2 (*cobA*) and sirohydrochlorin (*sirC*) with the nickel chelatase (*cfbA/cbiX*^{S}) by cloning them consecutively on the same plasmid to give pETcoco-2-*cobA*-*sirC*-*cfbA*. Additionally, to maximise the availability of Ni^{2+} for CfbA, we added the gene for the *Helicobacter pylori* nickel transporter (*nixA*)[23] to the construct to give pETcoco-2-*cobA*-*sirC*-*cfbA*-*nixA*. *E. coli* cells containing pETcoco-2-*cobA*-*sirC*-*cfbA* grown in the presence of nickel, at concentrations between 25 μM and 100 μM, were dark brown in colour. However, *E. coli* containing pETcoco-2-*cobA*-*sirC*-*cfbA*-*nixA* grown under the same conditions were observed to have a dark violet pigmentation (Extended Data Figure 1). The violet pigment was identified as Ni^{2+}-sirohydrochlorin by mass spectrometry (Extended Data Figure 2). Altogether, these results show that CfbA/CbiX^{S} can act as a nickel-chelatase both *in vitro* and *in vivo*. Given the large accumulation of Ni^{2+}-sirohydrochlorin within the recombinant *E. coli*, several milligrams per litre of culture, and the lack of free sirohydrochlorin, we can state that CfbA is more than active enough *in vivo* to support F_{430} synthesis. The discrimination between metals such as Ni^{2+} and Co^{2+} *in vivo* by the chelatase must reflect the different availabilities of these divalent metal ions in the bacterial cytoplasm[24].

Amidase CfbE

To investigate the *in vivo* activity of the putative *a,c*-diamide synthetase (amidotransferase or amidase), CfbE (Mbar_A0348), we co-transformed *E. coli* with the CfbE-producing plasmid pET14b-*cfbE* and pETcoco-2-*cobA*-*sirC*-*cfbA*-*nixA*. The resulting strain was grown in the presence of exogenous nickel and was harvested as a dark violet pellet. Extraction of the His_6-tagged CfbE by IMAC from the lysed cell pellet resulted in the co-isolation of a tightly bound violet coloured pigment (Extended Data Figure 2) in line with the observation that many tetrapyrrole biosynthetic enzymes bind their products tightly in order to facilitate direct metabolite channelling[25]. Analysis of this pigment by HPLC-MS revealed that it elutes as a single peak at 20.5 min with a mass of 917 Da, consistent with the expected molecular weight for Ni^{2+}-sirohydrochlorin diamide ($C_{42}H_{46}N_6O_{14}Ni$). In comparison, a standard of Ni^{2+}-sirohydrochlorin ($C_{42}H_{44}N_4O_{16}Ni$) eluted on HPLC-MS as a triple peak between 23-25 min with the predominant species showing a mass of 919 Da (Extended Data Figure 2).

The amidase activity of CfbE was investigated by incubating purified enzyme with Ni^{2+}-sirohydrochlorin, MgATP and glutamine. HPLC-MS analysis of the reaction products showed a single peak at 20.5 min with a mass of 917 Da (Extended Data Figure 2). By replacing glutamine with $^{15}NH_3$ in the CfbE reaction, it was found that the main product peak eluted at the same retention time, but exhibited an increased mass of two units to 919 Da, consistent with the incorporation of the heavy isotope into the tetrapyrrole side chains during the reaction (Extended Data Figure 2). NMR analysis of Ni^{2+}-sirohydrochlorin *a,c*-diamide after labelling of the side chains with $^{15}NH_3$ confirmed the incorporation of the two amide groups into the acetic acid side chains attached to rings A and B (Extended Data Figures 2 and 3; Supplementary Information Table 1).

Single turnover reactions demonstrated that the order of side chain amidation was random whilst time course studies indicated a direct conversion of the substrate into the diamide product, without release of the monoamide. Sirohydrochlorin also acted as a substrate for CfbE but only produced a monoamide species in a much slower reaction, highlighting that Ni^{2+}-sirohydrochlorin is the preferred substrate for the amidotransferase.

Finally, kinetic parameters were determined for the amidation reaction from a study of both the ATPase and glutaminase activities of CfbE in the presence of Ni^{2+}-sirohydrochlorin (Extended Data Figure 4). With glutamine as the variable substrate and ATP fixed at 0.5 mM, the K_m and turnover number were estimated at 46 μM and 0.78 min^{-1}, respectively. When the concentration of ATP was varied, with glutamine fixed at 1 mM, K_m and turnover number were estimated at 28 μM and 1.03 min^{-1}, respectively. Further, the enzyme was found to be inactive with other metallo-sirohydrochlorins such as siroheme and Co^{2+}-sirohydrochlorin.

Reductase CfbC/D

The CfbC/D proteins (Mbar_A0346, Mbar_A0347) belong to the family of the so-called class IV nitrogenase NflD/H[26,27] that was shown to lack nitrogenase activity in *Methanocaldococcus jannaschii* but was suspected of being involved in a methanogen specific process[18]. Recombinant CfbC and CfbD were produced as His_6-tagged proteins in *E. coli* and purified under anaerobic conditions, but UV/Vis absorption spectra and iron and sulfide determination assays indicated that Fe-S cluster incorporation were very low (<0.5 mol of iron and about 1 mol of sulfide per mol of protein). These values were improved through chemical Fe-S cluster reconstitution. The resulting iron and sulfide contents suggested the presence of inter-subunit [4Fe-4S] clusters. Consistent with this, both CfbC and CfbD migrated as dimers during gel filtration chromatography, although CfbD migrated as a monomer in the absence of the cluster. The presence of [4Fe-4S] centres on dithionite

reduced CfbC/D was confirmed by EPR spectroscopy, where features in the g = 4 and g = 2 regions arise from the S = 3/2 and S = ½ spin states of $[4Fe\text{-}4S]^{1+}$ clusters present in both proteins (Figure 2). Although CfbC is insensitive to the presence of MgATP, CfbD shows both MgADP and MgATP-dependent changes in the S = ½ and S = 3/2 signals (Figure 2, ii-iv). In mixtures of CfbC and CfbD the S = ½ signal for CfbD is much more intense than that of CfbC at the same protein concentration (Figure 2, vii), suggesting that CfbC has the lower midpoint redox potential (E_M) and hence the need for ATP-coupled 'uphill' electron transfer. The addition of MgATP to the protein mixtures produces the spectrum of Figure 2, viii, showing a greater reduction of CfbC and less reduced CfbD in keeping with the proposed MgATP-dependent electron transfer from CfbD to CfbC.

The reductase activity was investigated by incubating reconstituted CfbC/D with Ni^{2+}-sirohydrochlorin *a,c*-diamide, MgATP and sodium dithionite as the source of electrons. During the incubation, the characteristic UV/Vis absorbance of Ni^{2+}-sirohydrochlorin *a,c*-diamide at 594 nm decreased, and new absorption features around 446 and 423 nm appeared (Figure 3). Interestingly, the decrease in absorbance at 594 nm and the concomitant increase in absorbance at 446 nm were observed only during the first 1.5 h of incubation, and the absorption feature at 446 nm shifted to 423 nm during prolonged incubation for 14-22 h without any further signal decrease at 594 nm. When CfbC or MgATP were omitted from the assay as a control, the UV/Vis absorption spectrum did not change (Figure 3).

HPLC analysis of the tetrapyrrole content of the CfbC/D assay mixture after 1.5 and 22 h of incubation revealed that the respective reaction products eluted at the same retention time but exhibited clearly different UV/Vis absorption spectra (Figure 3). Whereas the product formed after 1.5 h exhibited absorption features at 309, 358 and 446 nm, which is very similar to the spectrum of a synthetic Ni^{2+}-tetrahydrocorphinat[28], the product formed after 22 h showed absorption at 305 and 428 nm, strikingly similar to the absorption spectrum of *seco*-F_{430}[15]. Both reaction products exhibited a mass of 923 Da consistent with the theoretical mass of Ni^{2+}-hexahydrosirohydrochlorin *a,c*-diamide or *seco*-F_{430} (Extended Data Figure 5). Together these results suggest that during the first part of the reaction (1.5 h) CfbC/D reduces the macrocycle through the addition of 6 electrons and 7 protons. The subsequent reaction (22 h), which may be spontaneous[15,29,30], represents lactam formation on ring E and the generation of *seco*-F_{430}. Indeed, the structure of the *seco*-F_{430} intermediate was confirmed using 2D heteronuclear NMR spectroscopy in D_2O (Extended Data Figure 6; Supplementary Information Table 2). The overall effect of the reduction process and ring lactamisation is to introduce 7 new steric centres into the macrocycle, indicating that the CfbC/D catalyses a highly orchestrated spatial and regio-selective reaction.

It is interesting to note that Nature employs nitrogenase-like proteins (NifD, H, K) to catalyse difficult reduction reactions, or at least reactions that require a low redox potential, including the reduction of N_2 to NH_3[31], protochlorophyllide to chlorophyllide[26] and Ni^{2+}-sirohydrochlorin diamide to Ni^{2+}-hexahydrosirohydrochlorin diamide. Clearly, the role of CfbC/D more closely parallels the stereospecific reduction of the C17-C18 double bond catalysed by the orthologous DPOR during chlorophyll and bacteriochlorophyll biosynthesis[26], but the requirement in F_{430} biosynthesis for only the NifD and NifH homologues suggests that this system may provide a simpler model for the coupling of ATP hydrolysis to such biological reduction processes. Significantly, we have yet to identify the source of the electrons, such as a ferredoxin, for the saturation of the three double bonds during F_{430} biosynthesis, an omission that may hinder the heterologous production of the coenzyme in *E. coli*.

seco to F_{430} by CfbB

To investigate the function of recombinant, purified CfbB (Mbar_A0345), the protein was added to an assay mixture containing either Ni^{2+}-hexahydrosirohydrochlorin *a,c*-diamide formed by the action of CfbC/D or *seco*-F_{430} together with MgATP. At different time points, the tetrapyrrole content of the mixtures was analysed by HPLC with diode-array detection and HPLC-MS. As shown in Figure 4, CfbB converted both substrates into new reaction products as indicated by the changes of the characteristic UV/Vis absorption spectra. For the mixture containing the Ni^{2+}-hexahydrosirohydrochlorin *a,c*-diamide the major absorption peak at 446 nm slightly shifted to 448 nm and the features at 309 and 358 nm disappeared. For the reaction mixture containing *seco*-F_{430} the newly formed product exhibited absorption features identical to those of authentic coenzyme F_{430} with maxima at 276 and 436 nm (Figure 3 and Extended Data Figure 7). For both reaction products, HPLC-MS revealed a mass of 905 Da, consistent with the theoretical mass of coenzyme F_{430} (Extended Data Figure 7). Considering the different absorption spectra, we propose that CfbB converts Ni^{2+}-hexahydrosirohydrochlorin *a,c*-diamide into a coenzyme F_{430} variant lacking the lactam ring E and *seco*-F_{430} into coenzyme F_{430}. Further activity assays with less CfbB showed that the conversion of *seco*-F_{430} occurs much faster than that of Ni^{2+}-hexahydrosirohydrochlorin *a,c*-diamide establishing *seco*-F_{430} as the true substrate for CfbB.

The structure of coenzyme F_{430} formed by CfbB was confirmed by 2D heteronuclear NMR spectroscopy. It was not possible to obtain a complete data set for coenzyme F_{430} in D_2O as the ROESY and HMBC spectra were of poor quality. Therefore, we used the non-coordinating solvent TFE-d_3, which allowed us to assign all resonances and thereby confirm the structure.. Cyclisation of the ring D propionate side chain was confirmed through absence of a proton at the C10 position and the carbon chemical shift of $C17^3$ observed at 200.34 ppm. The chemical shifts were in close agreement with previously published data

(Extended Data Figure 8; Supplemental Information Table 3)[32]. A mechanism for CfbB is shown in Extended Data Figure 9.

Conclusion

The elucidation of the pathway for coenzyme F_{430} biosynthesis (Figure 5) completes our understanding of how the major members of the modified tetrapyrrole family are constructed. By using a rich tapestry of enzymes Nature has shown how it is possible to construct a broad range of complex small molecules, such as heme, chlorophyll, vitamin B_{12} and coenzyme F_{430}, that are all derived from a common tetrapyrrole template and which are all involved in fundamental cellular processes, ranging from photosynthesis through to respiration. Although the biosynthesis of molecules such as heme and chlorophyll have been understood for some time[12] recent research has led to the determination of the aerobic[25,33] and anaerobic[34] pathways for vitamin B_{12} biosynthesis and the unexpected discovery of alternative routes for heme synthesis[35,36]. By identifying the enzymes responsible for the transformation of sirohydrochlorin into coenzyme F_{430} we have been able to show how the assembly of the molecular framework that is used to house nickel is orchestrated and optimised for its role in methanogenesis. Three of these biosynthetic steps require MgATP reflecting the high energetic cost in making this specialised metallo-prosthetic group. Our understanding of F_{430} synthesis will not only allow the opportunity to explore the development of recombinant MCR systems, a key component of which requires the synthesis of the essential F_{430} coenzyme, but also lead to mechanistic studies of some very interesting enzymes.

Supplementary Information is linked to the online version of the paper at www.nature.com/nature.

Acknowledgments. We thank Maria Höninger, Tobias Schnitzer and Judith Streif for conducting initial experiments with CfbA and CfbC/D. We thank Prof. Dr. Rolf Thauer and Dr. Seigo Shima for the gift of the F_{430} standard. This work was supported by grants from the Boehringer Ingelheim Foundation (Exploration Grant) and the Deutsche Forschungsgemeinschaft (LA2412/6-1) to GL and from the Biotechnology and Biological Sciences Research Council (BBSRC; 68/B19356 and BB/I012079) to MJW.

Author Contributions: SJM, STS, CS, ED, ADL, JVR, SB and CB all undertook aspects of the experimental work, cloning, protein purification and enzyme assays, and helped with the interpretation of the data. PTC provided the *nixA* clone and helped design the nickel uptake system. MJH, SJM and ADL designed and interpreted the NMR experiments and SEJR,

together with SJM, provided the EPR data. SJM, MJW and GL designed the experiments and wrote the paper.

Author Information: Reprints and permissions information is available at www.nature.com/reprints. The authors have no competing financial interests with this research. Correspondence and requests for materials should be addressed to m.j.warren@kent.ac.uk.

References

1 Ragsdale, S. W. Biochemistry of methyl-coenzyme M reductase: the nickel metalloenzyme that catalyzes the final step in synthesis and the first step in anaerobic oxidation of the greenhouse gas methane. *Met Ions Life Sci* **14**, 125-145 (2014).

2 Thauer, R. K. Biochemistry of methanogenesis: a tribute to Marjory Stephenson. 1998 Marjory Stephenson Prize Lecture. *Microbiology* **144**, 2377-2406 (1998).

3 Raghoebarsing, A. A. *et al.* A microbial consortium couples anaerobic methane oxidation to denitrification. *Nature* **440**, 918-921 (2006).

4 Scheller, S., Goenrich, M., Boecher, R., Thauer, R. K. & Jaun, B. The key nickel enzyme of methanogenesis catalyses the anaerobic oxidation of methane. *Nature* **465**, 606-608 (2010).

5 Shima, S. *et al.* Structure of a methyl-coenzyme M reductase from Black Sea mats that oxidize methane anaerobically. *Nature* **481**, 98-101 (2012).

6 Krüger, M. *et al.* A conspicuous nickel protein in microbial mats that oxidize methane anaerobically. *Nature* **426**, 878-881 (2003).

7 Ermler, U., Grabarse, W., Shima, S., Goubeaud, M. & Thauer, R. K. Crystal structure of methyl-coenzyme M reductase: the key enzyme of biological methane formation. *Science* **278**, 1457-1462 (1997).

8 Wongnate, T. & Ragsdale, S. W. The reaction mechanism of methyl-coenzyme M reductase: how an enzyme enforces strict binding order. *J Biol Chem* **290**, 9322-9334 (2015).

9 Wongnate, T. *et al.* The radical mechanism of biological methane synthesis by methyl-coenzyme M reductase. *Science* **352**, 953-958 (2016).

10 Thauer, R. K. & Bonacker, L. G. Biosynthesis of coenzyme F_{430}, a nickel porphinoid involved in methanogenesis. *Ciba Found Symp* **180**, 210-222 (1994).

11 Gilles, H. & Thauer, R. K. Uroporphyrinogen III, an intermediate in the biosynthesis of the nickel-containing factor F_{430} in *Methanobacterium thermoautotrophicum*. *Eur J Biochem* **135**, 109-112 (1983).

12 Warren, M. J. & Scott, A. I. Tetrapyrrole assembly and modification into the ligands of biologically functional cofactors. *Trends Biochem Sci* **15**, 486-491 (1990).

13 Färber, G. *et al.* Coenzyme F430 from Methanogenic Bacteria - Complete Assignment of Configuration Based on an X-Ray-Analysis of 12,13-Diepi-F430 Pentamethyl Ester and on NMR-Spectroscopy. *Helv Chim Acta* **74**, 697-716 (1991).

14 Mucha, H., Keller, E., Weber, H., Lingens, F. & Trosch, W. Sirohydrochlorin, a Precursor of Factor-F_{430} Biosynthesis in *Methanobacterium thermoautotrophicum*. *Febs Lett* **190**, 169-171 (1985).

15 Pfaltz, A., Kobelt, A., Huster, R. & Thauer, R. K. Biosynthesis of coenzyme F_{430} in methanogenic bacteria. Identification of $15,17^{(3)}$-*seco*-F_{430}-$17^{(3)}$-acid as an intermediate. *Eur J Biochem* **170**, 459-467 (1987).

16 Brindley, A. A., Raux, E., Leech, H. K., Schubert, H. L. & Warren, M. J. A story of chelatase evolution: identification and characterization of a small 13-15-kDa "ancestral" cobaltochelatase ($CbiX^S$) in the archaea. *J Biol Chem* **278**, 22388-22395 (2003).

17 Yan, Y. *et al.* Crystal structure of *Escherichia coli* UDPMurNAc-tripeptide d-alanyl-d-alanine-adding enzyme (MurF) at 2.3 A resolution. *J Mol Biol* **304**, 435-445 (2000).

18 Staples, C. R. *et al.* Expression and association of group IV nitrogenase NifD and NifH homologs in the non-nitrogen-fixing archaeon *Methanocaldococcus jannaschii*. *J Bacteriol* **189**, 7392-7398 (2007).

19 Warren, M. J., Raux, E., Schubert, H. L. & Escalante-Semerena, J. C. The biosynthesis of adenosylcobalamin (vitamin B_{12}). *Nat Prod Rep* **19**, 390-412 (2002).

20 Chivers, P. T. Nickel recognition by bacterial importer proteins. *Metallomics* **7**, 590-595 (2015).

21 Eitinger, T. & Mandrand-Berthelot, M. A. Nickel transport systems in microorganisms. *Arch Microbiol* **173**, 1-9 (2000).
22 Mulrooney, S. B. & Hausinger, R. P. Nickel uptake and utilization by microorganisms. *FEMS Microbiol Rev* **27**, 239-261 (2003).
23 Chivers, P. T., Benanti, E. L., Heil-Chapdelaine, V., Iwig, J. S. & Rowe, J. L. Identification of Ni-(L-His)$_2$ as a substrate for NikABCDE-dependent nickel uptake in *Escherichia coli*. *Metallomics* **4**, 1043-1050 (2012).
24 Waldron, K. J., Rutherford, J. C., Ford, D. & Robinson, N. J. Metalloproteins and metal sensing. *Nature* **460**, 823-830 (2009).
25 Deery, E. *et al.* An enzyme-trap approach allows isolation of intermediates in cobalamin biosynthesis. *Nat Chem Biol* **8**, 933-940 (2012).
26 Bröcker, M. J. *et al.* Crystal structure of the nitrogenase-like dark operative protochlorophyllide oxidoreductase catalytic complex (ChlN/ChlB)$_2$. *J Biol Chem* **285**, 27336-27345 (2010).
27 Muraki, N. *et al.* X-ray crystal structure of the light-independent protochlorophyllide reductase. *Nature* **465**, 110-114 (2010).
28 Fässler, A. *et al.* Preparation and Properties of Some Hydrocorphinoid Nickel(II)-Complexes. *Helv Chim Acta* **65**, 812-827 (1982).
29 Schlingmann, G., Dresow, B., Ernst, L. & Koppenhagen, V. B. The Structure of Yellow Metal-Free and Cobalt-Containing Corrinoids. *Liebigs Ann Chem*, 2061-2066 (1981).
30 Schlingmann, G., Dresow, B., Koppenhagen, V. B., Becker, W. & Sheldrick, W. S. Structure of Yellow Metal-Free and Yellow Cobalt-Containing Corrinoids. *Angew Chem Int Edit* **19**, 321-322 (1980).
31 Lee, C. C., Ribbe, M. W. & Hu, Y. Cleaving the n,n triple bond: the transformation of dinitrogen to ammonia by nitrogenases. *Met Ions Life Sci* **14**, 147-176 (2014).
32 Won, H., Olson, K. D., Wolfe, R. S. & Summers, M. F. 2-Dimensional NMR-Studies of Native Coenzyme-F$_{430}$. *J Am Chem Soc* **112**, 2178-2184 (1990).
33 Battersby, A. R. How nature builds the pigments of life: the conquest of vitamin B$_{12}$. *Science* **264**, 1551-1557 (1994).
34 Moore, S. J. *et al.* Elucidation of the anaerobic pathway for the corrin component of cobalamin (vitamin B$_{12}$). *Proc Natl Acad Sci* **110**, 14906-14911 (2013).
35 Bali, S. *et al.* Molecular hijacking of siroheme for the synthesis of heme and d1 heme. *Proc Natl Acad Sci* **108**, 18260-18265 (2011).
36 Dailey, H. A., Gerdes, S., Dailey, T. A., Burch, J. S. & Phillips, J. D. Noncanonical coproporphyrin-dependent bacterial heme biosynthesis pathway that does not use protoporphyrin. *Proc Natl Acad Sci* **112**, 2210-2215 (2015).
37 McGoldrick, H. M. *et al.* Identification and characterization of a novel vitamin B$_{12}$ (cobalamin) biosynthetic enzyme (CobZ) from *Rhodobacter capsulatus*, containing flavin, heme, and Fe-S cofactors. *J Biol Chem* **280**, 1086-1094 (2005).
38 Flühe, L. *et al.* The radical SAM enzyme AlbA catalyzes thioether bond formation in subtilosin A. *Nat Chem Biol* **8**, 350-357 (2012).
39 Kühner, M. *et al.* The alternative route to heme in the methanogenic archaeon *Methanosarcina barkeri*. *Archaea* **2014**, 327637 (2014).
40 Schubert, H. L. *et al.* The structure of *Saccharomyces cerevisiae* Met8p, a bifunctional dehydrogenase and ferrochelatase. *EMBO J* **21**, 2068-2075 (2002).
41 Bartolommei, G., Moncelli, M. R. & Tadini-Buoninsegni, F. A method to measure hydrolytic activity of adenosinetriphosphatases (ATPases). *PLoS One* **8**, e58615 (2013).
42 Schanda, P., Kupce, E. & Brutscher, B. SOFAST-HMQC experiments for recording two-dimensional heteronuclear correlation spectra of proteins within a few seconds. *J Biomol NMR* **33**, 199-211 (2005).

Figure Legends

Figure 1. Coenzyme F_{430} and biosynthesis gene clusters in methanogens. (A) Coenzyme F_{430} structure showing the numbering of the pyrrole rings A-D, lactam ring E and cyclohexanone ring F, and the C- and N-atoms. **(B)** Coenzyme F_{430} biosynthesis (*cfb*) gene clusters identified in this study. Homologous genes are shown in the same colour. Gene designations below the arrows represent the original annotation. The genes are: *M. barkeri*: *cfbA* (Mbar_A0344), *cfbB* (Mbar_A0345), *cfbC* (Mbar_A0346), *cfbD* (Mbar_A0347), *cfbE* (Mbar_A0348); *M. conradii*: *cfbA* (MTC_0061), *cfbB* (MTC_0062), *cfbC* (MTC_0063), *cfbD* (MTC_0064), *cfbE* (MTC_0065); *M. intestinalis*: *cfbA* (H729_08045), *cfbB* (H729_08040), *cfbC* (H729_08035), *cfbD* (H729_08030), *cfbE* (H729_08025).

Figure 2. EPR characterization of CfbC/D. X band continuous wave EPR spectra of dithionite reduced proteins: (i), CfbC: (ii), CfbD: (iii), CfbD plus excess MgADP: (iv), CfbD plus excess MgATP. ii – iv have the same vertical scale, protein concentration and dithionite concentration. (v), CfbC: (vi), CfbD: (vii), one-to-one mixture of CfbC and CfbD: (viii), one-to-one mixture of CfbC and CfbD plus excess MgATP. v-viii have the same vertical scale, protein concentration and dithionite concentration. Experimental parameters: microwave power 0.5 mW, field modulation amplitude 7 G, temperature 15 K.

Figure 3. Enzymatic activity of CfbC/D. (A) Left, UV/Vis absorption spectra of the conversion of Ni^{2+}-sirohydrochlorin *a,c*-diamide (green line) to Ni^{2+}-hexahydrosirohydrochlorin *a,c*-diamide (blue line) catalysed by CfbC/D during 1.5 h and autocatalytic formation of the lactam ring E yielding seco-F_{430} (pink and red lines) during 14-22 h of incubation. Right, UV/Vis absorption spectra of the control reaction lacking CfbC. **(B)** HPLC analysis (left) of the reaction products from (A) after 1.5 and 22 h of incubation with diode-array detection (right). Characteristic absorption features of the reaction products are indicated.

Figure 4. Enzymatic activity of CfbB. (A) UV/Vis absorption spectra (after HPLC separation) of the substrate Ni^{2+}-hexahydrosirohydrochlorin *a,c*-diamide (blue line) and the reaction product observed after incubation with CfbB and ATP for 2 h (pink line). **(B)** UV/Vis absorption spectra (after HPLC separation) of the substrate *seco*-F_{430} (red line) and the reaction product observed after incubation with CfbB and ATP for 1 h (orange line).

Figure 5. Biosynthesis of coenzyme F_{430} from sirohydrochlorin. The overall series of reactions required for the transformation of sirohydrochlorin into coenzyme F_{430}. There are four enzymatic steps, requiring CfbA, E, C/D and B, as well as one spontaneous process (*in vitro*), which might be enzyme-catalysed *in vivo*. The formal chemical changes for each step are given below the arrows not reflecting required cofactors or enzymatic mechanisms. The introduced structural changes are highlighted in red.

Methods

Cloning of putative coenzyme F_{430} biosynthetic genes. Genomic DNA of *Methanosarcina barkeri* strain Fusaro DSM804 was provided by Prof. Dr. Rolf Thauer from the Max-Planck-Institute for Terrestrial Microbiology (Marburg, Germany). A list of the plasmids used in this work is given in Extended Data Table 1. Genes were PCR amplified using a forward primer containing NdeI or AseI and a reverse primer with both SpeI and BamHI restriction sites (see Extended Data Table 1). The SpeI site was added on the reverse primer for subsequent link and lock cloning[37]. PCR fragments were digested with the relevant restriction enzymes and ligated into the pET14b plasmid. Genes were sequenced by GATC Biotech (Konstanz, Germany) or Source BioScience LifeSciences (Nottingham, UK). For the subcloning of Mbar_A0344, the gene was PCR amplified from pET14b-*cfbA* using primers cbiX_AscI_fo and cbiX_SalI_re (Extended Data Table 1). The resulting PCR fragment was digested with AscI and SalI and ligated into the correspondingly digested vector pETDuet-1 (Novagen / Merck Millipore, Darmstadt, Germany). The gene Mbar_A0344 was then cut from this construct using the restriction enzymes NdeI and SalI and the purified fragment was ligated into the correspondingly digested plasmid pET22b (Novagen) yielding expression plasmid pET22b-*cfbA* (Extended Data Table 1). For cloning of multi-gene constructs, sequenced genes were transferred into pET3a (to remove the His_6-tag), then constructed piecewise by the link and lock cloning method[37] in the pETcoco-2^{KAN} plasmid.

Recombinant protein production and purification of His_6-tagged proteins. *E. coli* Rosetta pLysS was transformed with plasmids containing putative coenzyme F_{430} biosynthesis genes cloned into pET14b and selected on LB agar with 34 µg mL^{-1} chloramphenicol and 100 µg mL^{-1} ampicillin. For protein production, an overnight pre-culture was grown in LB medium for 16 h at 37 °C, 150 rpm. The next day 10 mL of pre-culture was transferred into 1-4 L of LB medium with 34 µg mL^{-1} chloramphenicol and 100 µg mL^{-1} ampicillin. The cells were grown at 37 °C, 150 rpm until an OD_{600} of 1.0 was reached. Protein production was induced with 0.4 mM IPTG and cells were left overnight at 19 °C with 150 rpm shaking. For increased production of iron-sulfur enzymes, 1 mM ammonium ferric citrate was added to the cultures at the induction stage. Proteins containing Fe-S clusters were purified in an anaerobic glovebox (Belle Technologies or Coy Laboratory Products), with O_2 levels at less than 2 ppm. All buffers and solutions were purged with argon prior to use in the glovebox. *E. coli* cultures were centrifuged at 5,180 × *g* at 4 °C for 20 min. Cells were then resuspended in 15 mL of binding buffer (20 mM Tris-HCl pH 8, 500 mM NaCl and 5 mM imidazole), followed by sonication under anaerobic conditions at 4 °C for 5 minutes with 10 and 30 second pulse and rest cycles, respectively. Cell lysates were centrifuged at 37,044 × *g* at 4 °C for 20 min. The supernatant was then purified using 5 mL of pre-charged

nickel chelated sepharose. This was then washed with 50 mL of binding buffer, followed by washing steps (25 mL) containing increasing concentrations of imidazole from 30 to 70 mM. Elution was performed with buffer containing 400 mM imidazole. Purified protein was desalted on a pre-packed PD-10 column equilibrated in buffer without imidazole.

Recombinant production and purification of non-tagged CfbA. *E. coli* Rosetta pLysS containing plasmid pET22b-*cfbA* was cultivated as described above with the exception that the induction of protein production with IPTG was initiated when the cells had reached an OD_{600} of about 0.4. After overnight cultivation the cells were harvested by centrifugation and the cell pellet from 1 L of culture was resuspended in 20 mL of buffer A (50 mM Tris-HCl, pH 8) containing 1 mM phenylmethylsulfonyl fluoride (PMSF). Cells were disrupted by sonication and the resulting cell lysate was centrifuged in an ultracentrifuge at 175,000 × *g* at 4 °C for 60 min. The soluble protein fraction was loaded onto a 1 mL HiTrap Q XL column (GE Healthcare) at a flow rate of 1 mL min^{-1}. The column was washed with 10 mL of buffer A and the bound proteins were then eluted using a linear NaCl gradient (0 – 400 mM NaCl in buffer A) developed over 20 mL. The CfbA-containing elution fractions were pooled, concentrated to 5 mL and then loaded onto a HiLoad 16/600 Superdex 75 prep grade column (GE Healthcare) equilibrated with 50 mM Tris-HCl, pH 8, 150 mM NaCl at a flow rate of 1 mL min^{-1}. The elution fractions containing CfbA were pooled and the buffer of the purified protein was exchanged inside the anaerobic chamber using a PD-10 column equilibrated with anaerobic test buffer (25 mM Tris-HCl, pH 8, 150 mM NaCl, 10 mM $MgCl_2$, 10 % (*v/v*) glycerol). The purified CfbA was stored at -80°C until further use.

Reconstitution of iron-sulfur clusters. The reconstitution of iron-sulfur clusters within CfbC and CfbD was performed as described previously[38]. After reconstitution, the excess of iron and sulfide was removed by centrifugation and subsequent passage of the protein solution through a NAP-25 column (GE Healthcare) which was used according to the manufacturer's instructions. The iron and sulfide concentrations for Mbar_A0346 (CfbC) and Mbar_A0347 (CfbD) were determined as previously described[39]. Protein concentration was estimated separately using Bradford reagent (Bio-Rad Laboratories) with bovine serum albumin as a calibration standard.

EPR of CfbC and CfbD. Samples were prepared and then flash frozen in liquid nitrogen. EPR experiments were performed on a Bruker ELEXSYS E500 spectrometer operating at X-band, employing a Super High Q cylindrical cavity (Q factor ~ 16,000) equipped with an Oxford Instruments ESR900 liquid helium cryostat linked to an ITC503 temperature controller. Experimental parameters: microwave power 0.5 mW, field modulation amplitude 7 G, field modulation frequency 100 KHz, temperature 15 K.

Nickel chelatase activity assay (CfbA). Sirohydrochlorin was synthesized using the one-pot incubation method described previously[40]. For the CfbA activity assay, 5 µM sirohydrochlorin and 50 µM of $NiSO_4$ were incubated at 37°C with varying amounts of purified CfbA (0, 1, 1.5 and 2.5 µM) in anaerobic test buffer (50 mM Tris-HCl, pH 8, 150 mM NaCl, 10 mM $MgCl_2$, 10 % (v/v) glycerol) inside the anaerobic chamber. For each enzyme concentration the assay was performed at least three times. The deduced specific activity represents the mean value of all measurements. The chelation of nickel into sirohydrochlorin was monitored by recording UV/Vis absorption spectra at different time points using a V-650 spectrophotometer (Jasco, Gross-Umstadt, Germany).

Synthetic production of nickel-sirohydrochlorin *a,c*-diamide in *E. coli*. *E. coli* KRX auto-induction strain was transformed with the pETcoco-2^{KAN}-*cobA-sirC-cbiX*^{S}-*nixA* and pET14b-Mbar_A0348 plasmids using 0.2% (w/v) glucose to maintain the single copy state of the pETcoco-2^{KAN} derived plasmid and 25 µg mL^{-1} kanamycin and 100 µg mL^{-1} ampicillin for antibiotic selection. An overnight pre-culture was grown for 16 h at 28 °C, 150 rpm. The next day 10 mL of pre-culture was transferred into 1 L of 2YT medium with 50 µg mL^{-1} kanamycin, 100 µg mL^{-1} ampicillin, 0.05% glucose (w/v), 0.1% rhamnose (w/v), 0.01% (w/v) arabinose and between 25 µM and 100 µM $NiCl_2.6H_2O$. The cells were grown at 28 °C and 150 rpm for 24 h. This yields approximately 1-2 mg L^{-1} of nickel-sirohydrochlorin *a*,*c*-diamide in complex with the His_6-tagged amidotransferase Mbar_A0348 (CfbE) enzyme, which can be purified using IMAC purification under low-salt (100 mM) buffer conditions.

Amidotransferase kinetics (CfbE). The protocol for the antimony-phosphomolybdate colorimetric based stopped-assay[41] was used for determining the ATPase activity of the *M. barkeri* CfbE amidotransferase in the presence of its substrate nickel-sirohydrochlorin. 0.2% (w/v) citric acid was added after a time delay of 2 min to prevent background increases in absorbance from acid hydrolysis of ATP. Assays were performed in buffer B (20 mM Tris-HCl, pH 8 and 100 mM NaCl buffer) at 20 °C.

Amide ^{15}N labelling ATP titration experiment and NMR of nickel-sirohydrochlorin *a,c*-diamide. $(^{15}NH_3)_2SO_4$ (Cambridge Isotope Laboratories) was used for labelling of the amide side chains. Single-turnover reactions were prepared in 10 mL of buffer B with 25 µM of pure *M. barkeri* CfbE, 25 µM nickel-sirohydrochlorin, 1 mM $MgCl_2$, 25 mM $(^{15}NH_3)_2SO_4$. Turnover was controlled by an ATP titration series of 0, 25, 50 and 100 µM. Reactions were left for 30 min at 37 °C. The reaction product was purified in d_6-DMSO in order to reduce proton solvent exchange to allow observation of the NH amide signals, which are barely detectable in D_2O or acidic (pH 5) 1:10 H_2O/D_2O mixtures. Two-dimensional datasets were collected including ^{1}H-^{15}N HSQC, ^{1}H-^{1}H NOESY and ^{1}H-^{15}N HSQC-TOCSY spectra. The ^{1}H-^{15}N

correlation spectra were collected by the SOFAST-HSQC method, which increases sensitivity using fast repetition rates[42]. This method resolved four clear amide peaks with no background signals (Extended Data Figure 2). These were correlated to show clear NOE through space interactions with the ring A and C propionate side chains as indicated in the ROESY and NOESY spectra (Extended Data Figure 3; Supplementary Information Table 1). This provides strong evidence for the positioning of the amide groups at the *a* and *c* positions, thus confirming the product of the CfbE amidation reaction as Ni^{2+}-sirohydrochlorin *a,c*-diamide.

LC-MS of nickel-sirohydrochlorin and nickel-sirohydrochlorin *a,c*-diamide. Samples (10-100 µL) were injected onto an Ace 5 AQ column (2.1 x 150 mm, 5 µm, Advanced Chromatography Technologies) that was attached to an Agilent 1100 series HPLC coupled to a micrOTOF-Q (Bruker) mass spectrometer and equipped with online diode array and fluorescence detectors and run at a flow rate of 0.2 mL min^{-1}. Tetrapyrroles were routinely separated with a linear gradient of acetonitrile in 0.1% TFA. Mass spectra were obtained using an Agilent 1100 liquid chromatography system connected to a Bruker micrOTOF II MS, using electro-spray ionisation in positive mode. UV/Vis absorption spectra were monitored by DAD-UV detection (Agilent Technologies).

Nickel-sirohydrochlorin *a,c*-diamide reductase activity assay (CfbC/D). The assay for testing the reductase activity of CfbC/D was performed under anaerobic conditions at 37°C in anaerobic test buffer (50 mM Tris-HCl, pH 8, 150 mM NaCl, 10 mM $MgCl_2$, 10 % (v/v) glycerol). The assay contained 10 µM nickel-sirohydrochlorin *a,c*-diamide (formed *in situ* by the action of CfbE), 10 µM CfbC, 10 µM CfbD, 3.2 mM ATP, 3.2 mM sodium dithionite and residual amounts of the enzymes HemB, HemC, HemD, CobA, SirC, CfbA and CfbE which were used for the formation of nickel-sirohydrochlorin *a,c*-diamide. The reaction was followed by UV/Vis absorption spectroscopy and by analysing the tetrapyrrole content of the assay mixtures after 0, 1.5, 14 and 22 h of incubation by HPLC. For HPLC analysis, the tetrapyrroles were extracted by denaturation of the proteins using guanidinium chloride. For this, 160 mg of guanidinium chloride were dissolved in 300 µL of the sample, and the mixture was incubated for 2 min at room temperature. Subsequently, the free tetrapyrroles were separated from the denatured proteins by ultrafiltration using an Amicon™ Ultra 10 k filter unit (Merck Millipore). The tetrapyrrole-containing filtrate (40 µL injection volume) was analysed by HPLC using a ReproSil-Pur C18 AQ column (Dr. Maisch HPLC GmbH, Ammerbuch-Entringen, Germany) and a JASCO HPLC 2000 series system (Jasco). The separation was carried out at a flow rate of 0.2 mL min^{-1}. Solvent A was 0.01 % formic acid in H_2O and solvent B was acetonitrile. Tetrapyrroles eluted with a linear gradient system within 25 min: start conditions 95 % A / 5 %B and end conditions 65 % A / 35 % B. The

tetrapyrroles were detected by photometric diode array analysis in the range of 220-670 nm. The masses of the eluting tetrapyrroles were confirmed by ESI-MS analysis on an Esquire 3000+ ESI ion trap mass spectrometer coupled to an Agilent 1100er series HPLC system using the same column, eluent, and gradient. Scan was carried out in alternating mode between *m/z* 500-2000, the target mass set to *m/z* 1000, nebulizer pressure to 70 psi, dry gas flow to 11 L min^{-1} and dry gas temperature to 360°C.

Ring F ligase activity assay (CfbB). The CfbB assay was conducted under anaerobic conditions at 37°C in anaerobic test buffer (50 mM Tris-HCl, pH 8, 150 mM NaCl, 10 mM $MgCl_2$, 10 % (v/v) glycerol). The assay contained 7.5 µM of either Ni^{2+}-hexahydrosirohydrochlorin *a,c*-diamide or *seco*-F_{430} (formed as described for the CfbC/D assay), 0.75 µM or 7.5 µM CfbB and 3.2 mM ATP. After 1 or 2 h of incubation, the tetrapyrroles were extracted and analysed by HPLC and HPLC-MS as described for the CfbC/D assay.

NMR of *seco*-F_{430}. For structural determination an isotopically enriched sample (4 mM) of the *seco*-F_{430} intermediate was prepared using ^{15}N-glutamine as the amide donor and the incorporation of two ^{15}N atoms in the product was confirmed by HPLC-MS. Analysis of the data following assignment established the presence of the lactam attached to ring B. This was determined from the combination of the following pieces of information. Protons attached to C3-C4 -C5 are present in a single scalar coupled network and C5 (36.37 ppm) appears sp^3 hybridised with two germinal protons (1.56 and 1.84 ppm). The chemical shift of C6, assigned from the ^{1}H-^{13}C HMBC spectrum, is 96.39 ppm. Lastly, the ^{15}N HSQC clearly shows 3 signals from which the germinal pair of protons was assigned to the NH_2 of the *a*-sidechain (N23) and the single N-H resonance observed at lower field to the lactam formed from the *c*-sidechain of ring B (N73) (Extended Data Figure 6).

Data availability statement. All data generated or analysed during this study are included in this published article (and its supplementary information files).

Extended Data Figure Legends

Extended Data Figure 1. Nickel chelatase activity of CfbA. (A) and (B) *In vitro* activity assay of CfbA. Purified CfbA was incubated with sirohydrochlorin and $NiSO_4$ at 37°C (A). The insertion of nickel was monitored by UV/Vis absorption spectroscopy every 15 min. When CfbA was omitted from the assay mixture (B), no nickel insertion was observed. **(C)** *In vivo* activity of CfbA. Cell pellets of *E. coli* cells transformed with either pETcoco-2-*cobA-sirC-cfbA* or pETcoco-2-*cobA-sirC-cfbA-nixA* grown in the presence of nickel.

Extended Data Figure 2. Amidotransferase activity of CfbE. (A) *In vivo* activity of CfbE. *E. coli* cells transformed with pETcoco-2-*cobA-sirC-cfbA-nixA* and pET14b-*cfbE* and grown in the presence of nickel produce a dark violet pigment that co-purifies with CfbE during IMAC. **(B) and (C)** ^{15}N labelling of nickel-sirohydrochlorin *a,c*-diamide. **(B)** Reverse-phase HPLC chromatogram of (i) nickel-sirohydrochlorin substrate, *m/z* = 919; (ii) unlabelled nickel-sirohydrochlorin *a,c*-diamide, *m/z* = 917; (iii) ^{15}N labelled nickel-sirohydrochlorin *a,c*-diamide, *m/z* = 919. **(C)** ^{15}N ^{1}H HSQC of an ATP limited titration with nickel-sirohydrochlorin, CfbE and $^{15}NH_3$. The *a* and *c* amide groups increase proportionally in intensity as the level of ATP increases.

Extended Data Figure 3. NMR characterisation of Ni^{2+}-sirohydrochlorin *a,c*-diamide. ^{1}H-^{13}C HSQC (A) and ^{1}H-^{15}N HSQC (B) of 4 mM Ni^{2+}-sirohydrochlorin *a,c*-diamide in D_2O.

Extended Data Figure 4. Steady-state kinetics of the *M. barkeri* CfbE amidotransferase with glutamine or ATP as a variable. (A) 1 mM glutamine with ATP varied between 0.05 – 1.5 mM ATP. **(B)** 0.5 mM ATP with glutamine varied between 0.05 – 10 mM. Fixed conditions: Buffer B, 20°C, 2.5 µM *M. barkeri* CfbE, 25 µM nickel-sirohydrochlorin, 5 mM $MgCl_2$. The mean values and error bars were calculated from 3 technical repeats.

Extended Data Figure 5. Characterization of the CfbC/D assay reaction products by mass spectrometry after HPLC separation. (A) Mass spectrum with the isotopic pattern of the reaction product after 1.5 h of incubation measured in positive ion mode. **(B)** Mass spectrum with the isotopic pattern of the reaction product after 22 h of incubation measured in positive ion mode.

Extended Data Figure 6. NMR characterization of *seco*-F_{430}. ^{1}H-^{13}C HSQC (A) and ^{1}H-^{15}N HSQC (B) of 4 mM *seco*-F_{430} in D_2O.

Extended Data Figure 7. Characterization of the CfbB assay reaction products. (A) UV/Vis absorption spectrum of an F_{430} standard in 0.01 % formic acid / acetonitrile. **(B)** CfbB assay with Ni^{2+}-hexahydrosirohydrochlorin *a,c*-diamide as the substrate. Mass spectrum with the isotopic pattern of the reaction product after 2 h of incubation measured in positive ion mode after HPLC separation. **(C)** CfbB assay with *seco*-F_{430} as the substrate. Mass spectrum with the isotopic pattern of the reaction product after 22 h of incubation measured in positive ion mode after HPLC separation.

Extended Data Figure 8. NMR characterisation of F_{430} synthesised by CfbB. ^{1}H-^{13}C HSQC and ^{1}H-^{15}N HSQC of F_{430} in TFE-d3.

Extended Data Figure 9. Proposed mechanism for the reaction catalyzed by CfbB. Initially, CfbB promotes the ATP-dependent phosphorylation of the propionic acid side chain on ring D of *seco*-F_{430}. This activated side chain is then able to undergo cyclisation to form ring F and thereby generate coenzyme F_{430}.

Extended Data Table 1. Plasmids and primers used in this study.

a

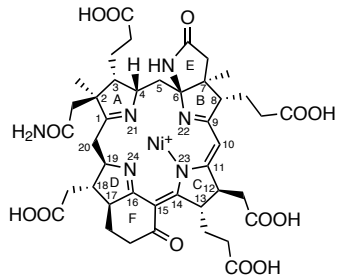

coenzyme F_{430}

b

Methanosarcina barkeri

Methanocella conradii

Methanomasiliicoccus intestinalis

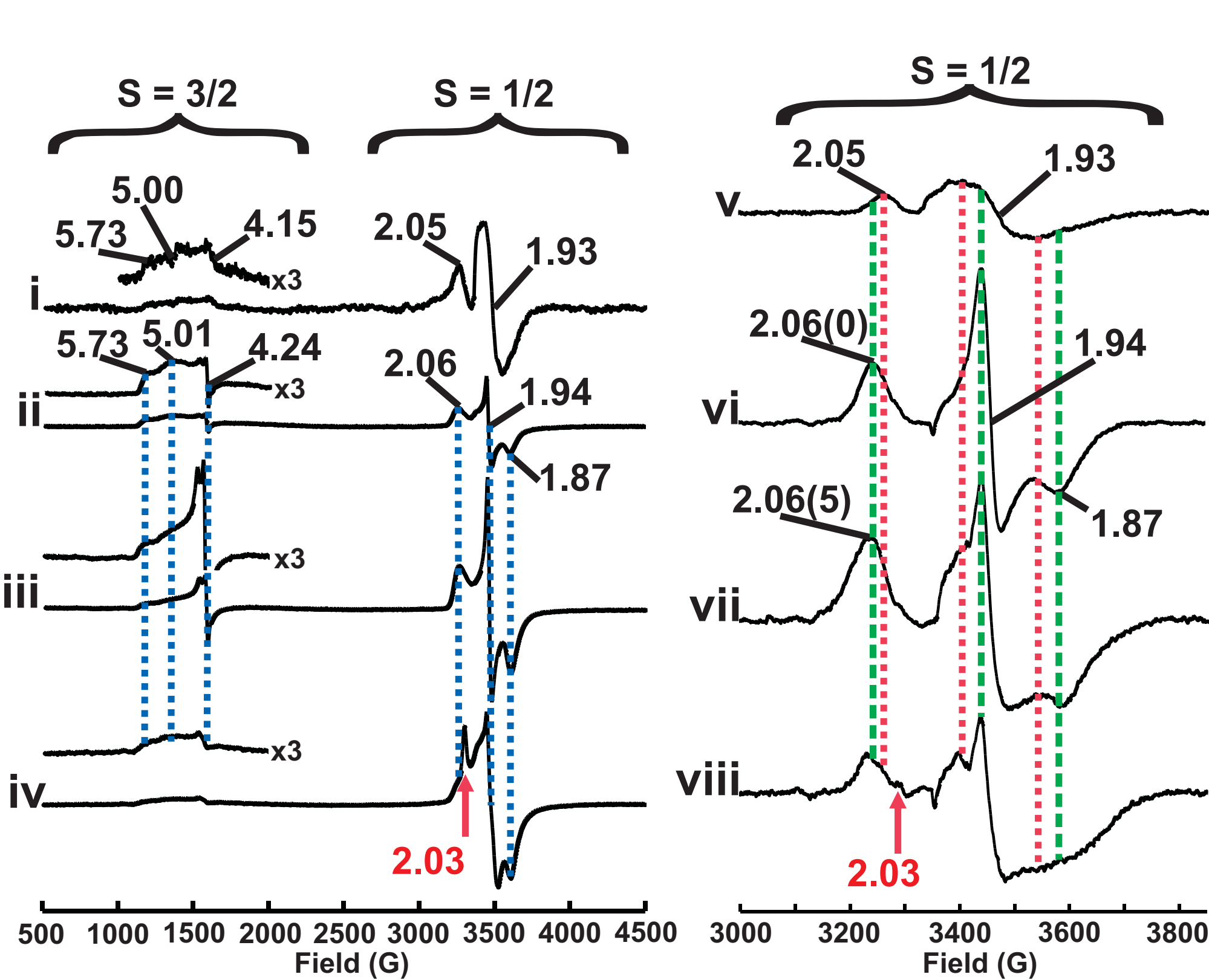
S = 3/2
S = 1/2
5.00
5.73
4.15
x3
2.05
1.93
i
5.73
5.01
4.24
x3
2.06
1.94
ii
1.87
x3
iii
x3
iv
2.03
500
1000
1500
2000
2500
3000
3500
4000
4500
Field (G)
S = 1/2
2.05
1.93
v
2.06(0)
1.94
vi
2.06(5)
1.87
vii
viii
2.03
3000
3200
3400
3600
3800
Field (G)

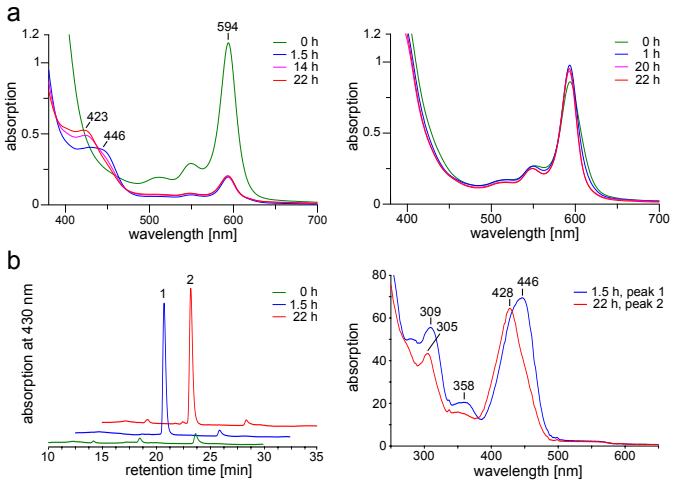
a
absorption
wavelength [nm]
0 h
1.5 h
14 h
22 h
423
446
594
0 h
1 h
20 h
22 h
b
absorption at 430 nm
retention time [min]
1
2
0 h
1.5 h
22 h
absorption
wavelength [nm]
309
305
358
428
446
1.5 h, peak 1
22 h, peak 2

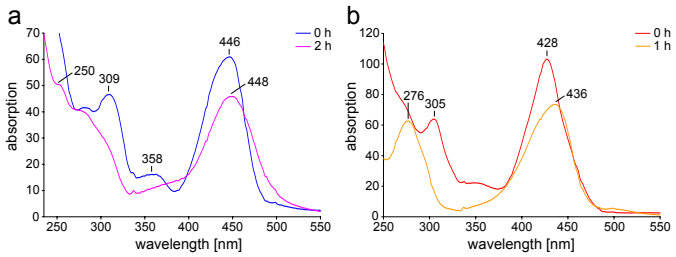
a
0 h
2 h
absorption
wavelength [nm]
250
309
358
446
448
b
0 h
1 h
absorption
wavelength [nm]
276
305
428
436

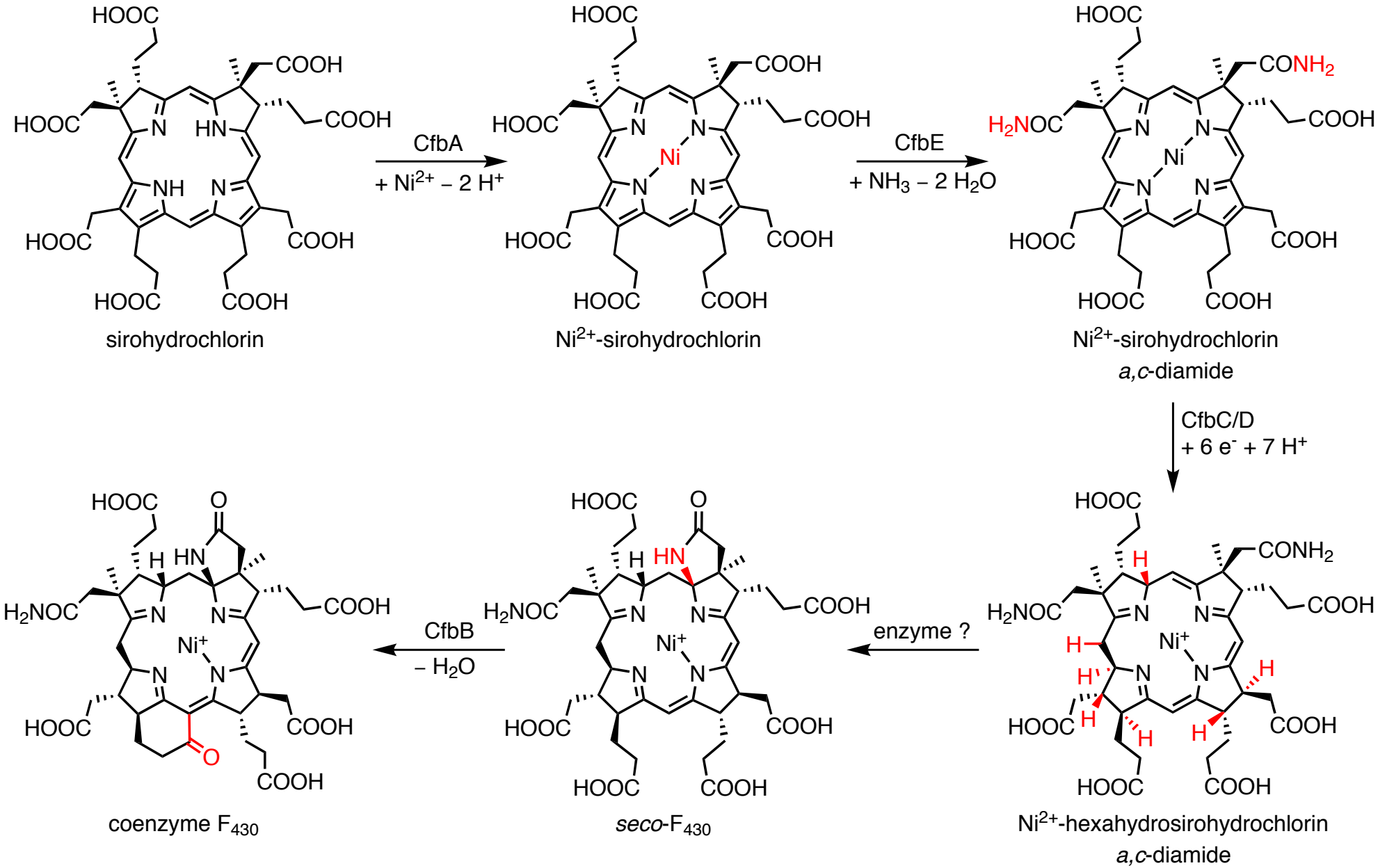
sirohydrochlorin
CfbA
+ Ni2+ – 2 H+
Ni2+-sirohydrochlorin
CfbE
+ NH3 – 2 H2O
Ni2+-sirohydrochlorin
a,c-diamide
CfbC/D
+ 6 e- + 7 H+
Ni2+-hexahydrosirohydrochlorin
a,c-diamide
enzyme ?
seco-F430
CfbB
– H2O
coenzyme F430

Plasmid	Source
pMH003 – Iron sulfur cluster (*isc*) biogenesis operon from *E. coli*	(*7*)
pET22b-*nixA* – Nickel transporter from *H. pylori*	This work
pETcoco-2^{KAN}	(*8*)
pETcoco-2^{KAN}-*cobA*	This work
pETcoco-2^{KAN}-*cobA-sirC*	This work
pETcoco-2^{KAN}-*cobA-sirC-cfbA*	This work
pETcoco-2^{KAN}-*cobA-sirC-cfbA-nixA*	This work
pET14b-*cfbA* (Mbar_A0344)	This work
pET14b-*cfbB* (Mbar_A0345)	This work
pET14b-*cfbC* (Mbar_A0346)	This work
pET14b-*cfbD* (Mbar_A0347)	This work
pET14b-*cfbE* (Mbar_A0348)	This work
pET14b-*cfbC-cfbD-isc*	This work
pET14b-*cfbD-cfbC-isc*	This work
pET22b-*cfbA*	This work
pET3a-*cobA*	This work
pET3a-*sirC*	This work
pET3a-*cfbA* (Mbar_A0344)	This work
pET3a-*nixA*	This work

Primer	Sequence	Site
MB0344 F	CACCATATGACAGAAAAACTCG	NdeI
MB0344 R	GTGGGATCCACTAGTTAAAGGGCTTCCTGAACC	BamHI/SpeI
MB0345 F	CACCATATGGACCTGTACCGGAAG	NdeI
MB0345 R	GTGGGATCCACTAGTTAACGGAAGCATTTTACC	BamHI/SpeI
MB0346 F	CACCATATGGCTGAAAAAGAGATTTC	NdeI
MB0346 R	GTGGGATCCACTAGTCAGGCTTCCTTTGCAAC	BamHI/SpeI
MB0347 F	CACATGAAAAACCAGAAGATC	NdeI
MB0347 R	GTGGGATCCACTAGTTATTTTGTTAATTCC	BamHI/SpeI
MB0348 F	CGCCATATGCTTAACGACAAGCAATCC	NdeI
MB0348 R	ATGGGATCCACTAGTTCACGGAAGAACCCTGG	BamHI/SpeI
cbiX_AscI_fo	TATAGGCGCGCCAAGAAGGAGATATACC	AscI
cbiX_SalI_re	TATAGTCGACTTAAAGGGCTTCCTGAACC	SalI

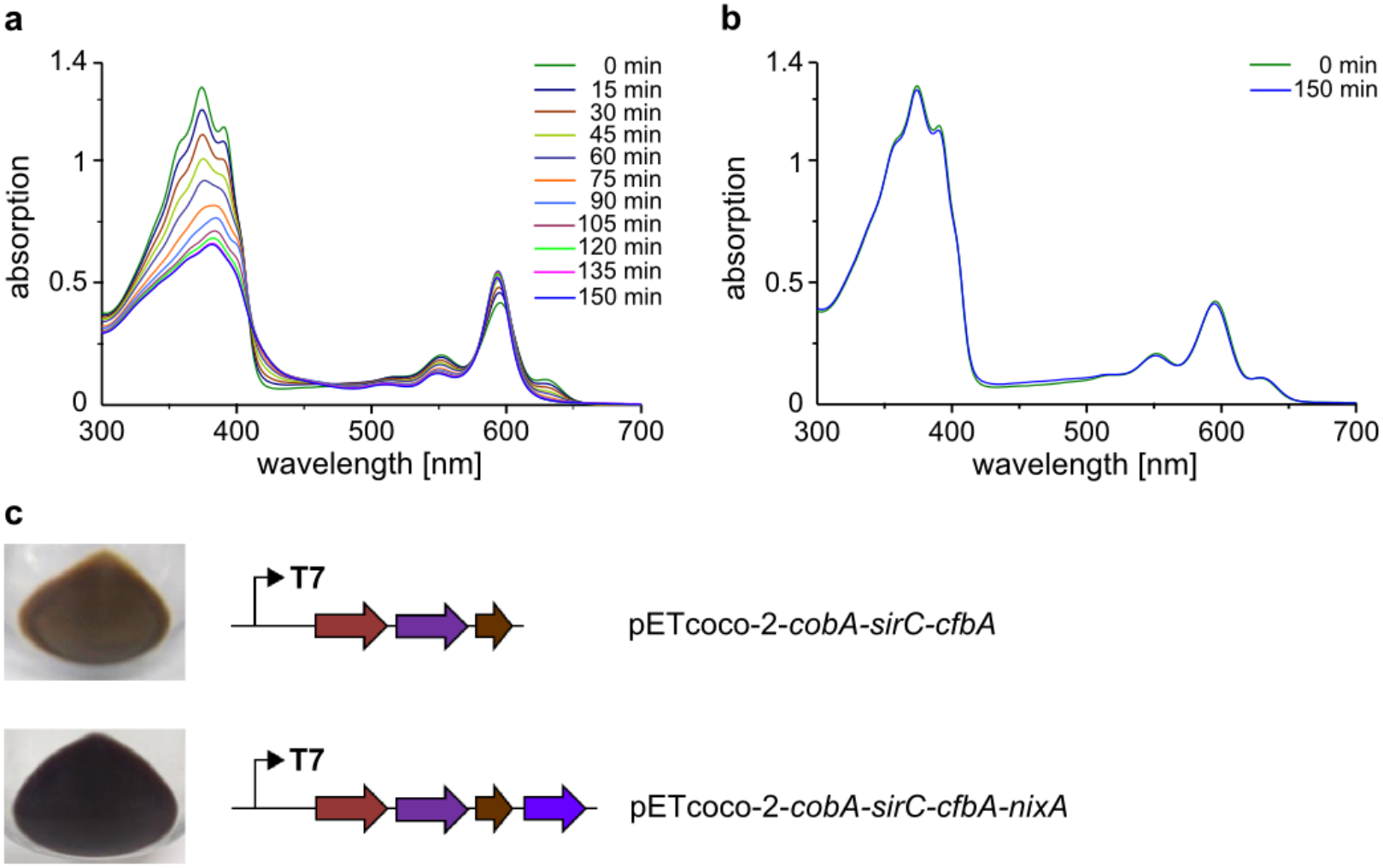
a
1.4
1
0.5
0
absorption
300
400
500
600
700
wavelength [nm]
0 min
15 min
30 min
45 min
60 min
75 min
90 min
105 min
120 min
135 min
150 min
b
1.4
1
0.5
0
absorption
300
400
500
600
700
wavelength [nm]
0 min
150 min
c
T7
pETcoco-2-cobA-sirC-cfbA
T7
pETcoco-2-cobA-sirC-cfbA-nixA

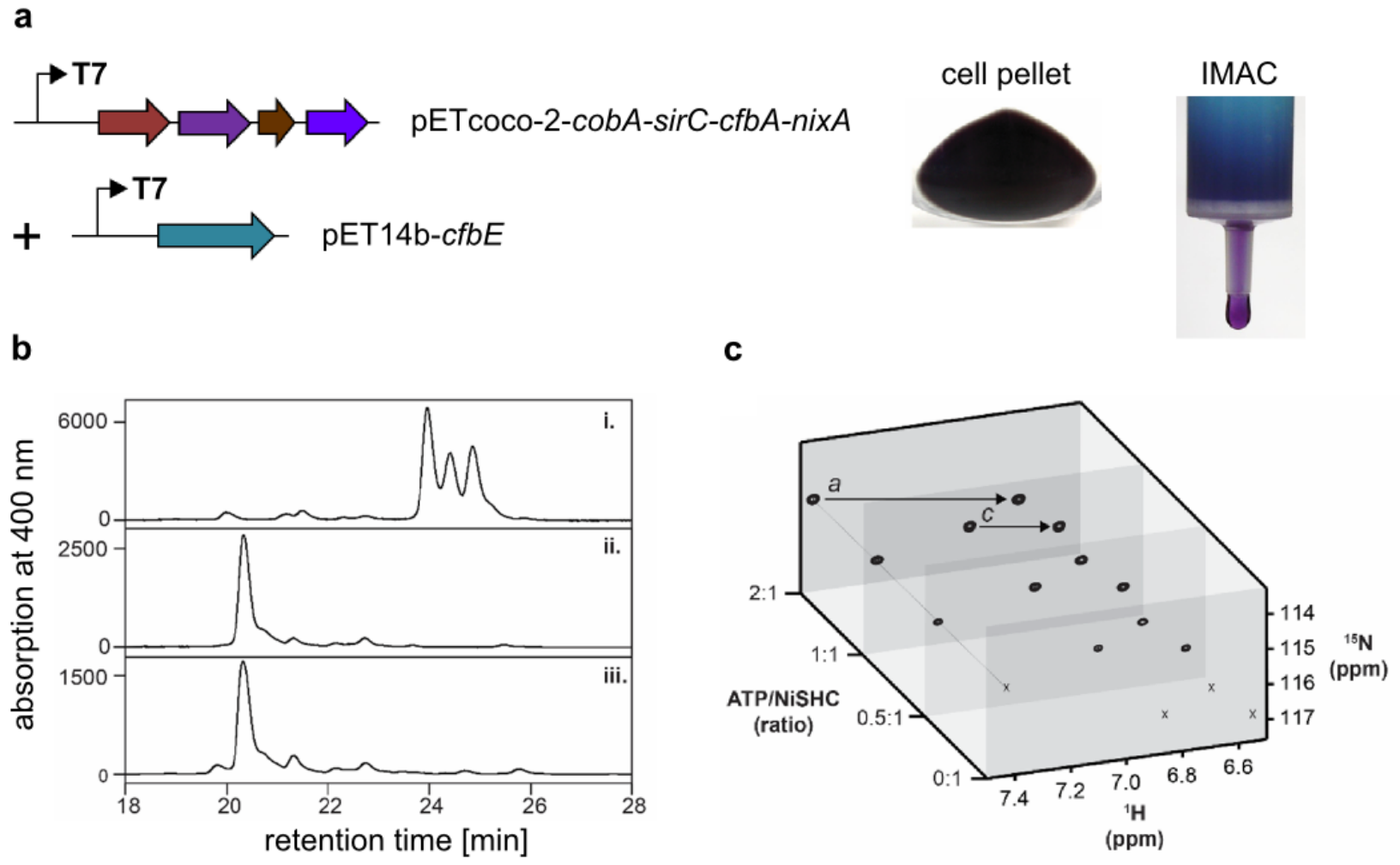
a
T7
pETcoco-2-cobA-sirC-cfbA-nixA
T7
+
pET14b-cfbE
cell pellet
IMAC
b
absorption at 400 nm
6000
0
i.
2500
0
ii.
1500
0
iii.
18
20
22
24
26
28
retention time [min]
c
a
c
2:1
1:1
0.5:1
0:1
ATP/NiSHC
(ratio)
7.4
7.2
7.0
6.8
6.6
1H
(ppm)
114
115
116
117
15N
(ppm)

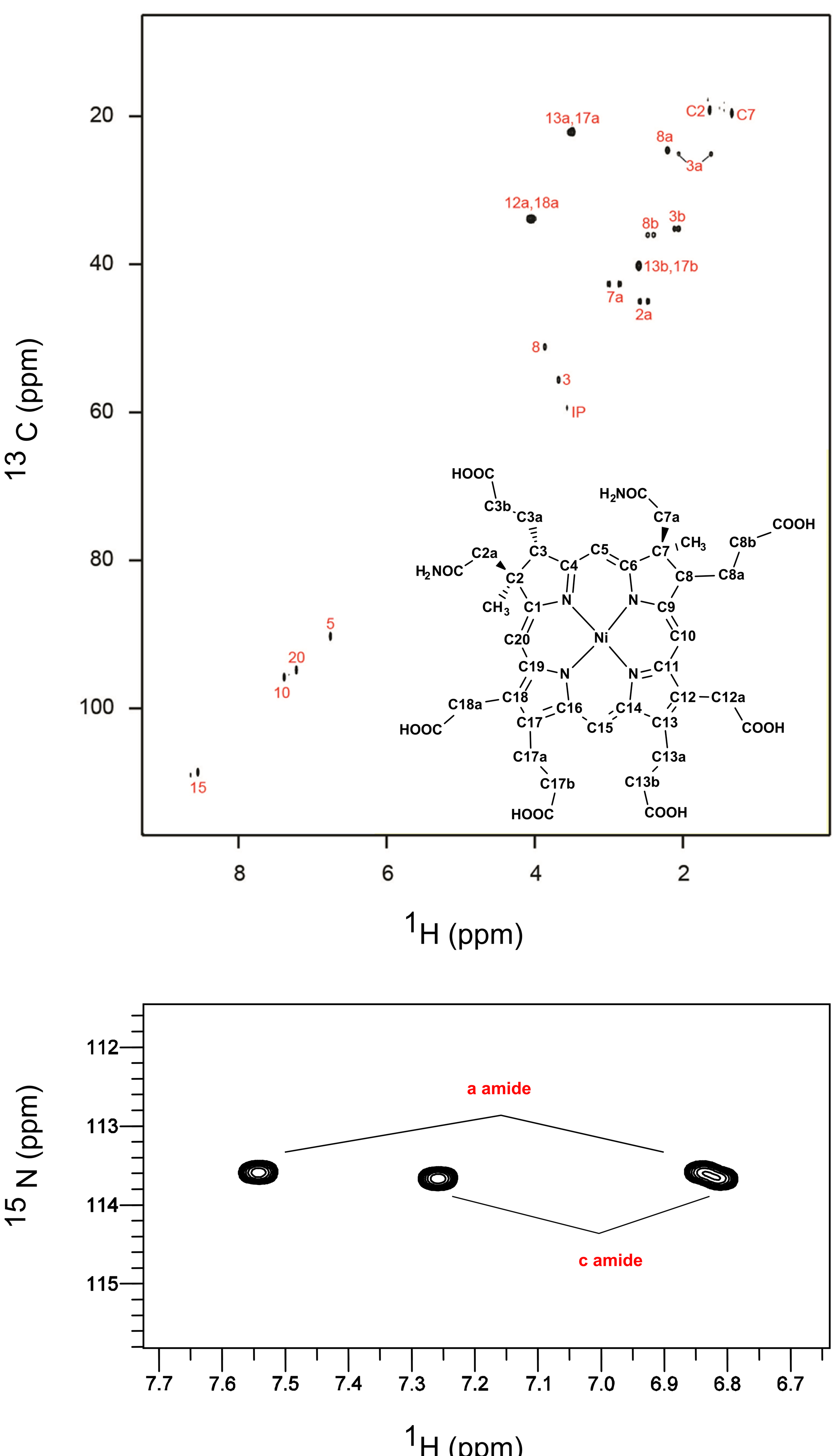
20
40
60
80
100
^{13}C (ppm)
13a,17a
C2
C7
8a
3a
12a,18a
8b
3b
13b,17b
7a
2a
8
3
IP
5
20
10
15
HOOC
C3b
C3a
H_2NOC
C7a
COOH
C8b
CH_3
C2a
C3
C5
C7
C4
C6
C8
C8a
C2
N
N
C1
C9
CH_3
Ni
C20
C10
C19
N
N
C11
C18
C16
C14
C12
C12a
C18a
C17
C15
C13
HOOC
COOH
C17a
C13a
C17b
C13b
HOOC
COOH
8
6
4
2
^{1}H (ppm)
112
113
114
115
^{15}N (ppm)
a amide
c amide
7.7
7.6
7.5
7.4
7.3
7.2
7.1
7.0
6.9
6.8
6.7
^{1}H (ppm)

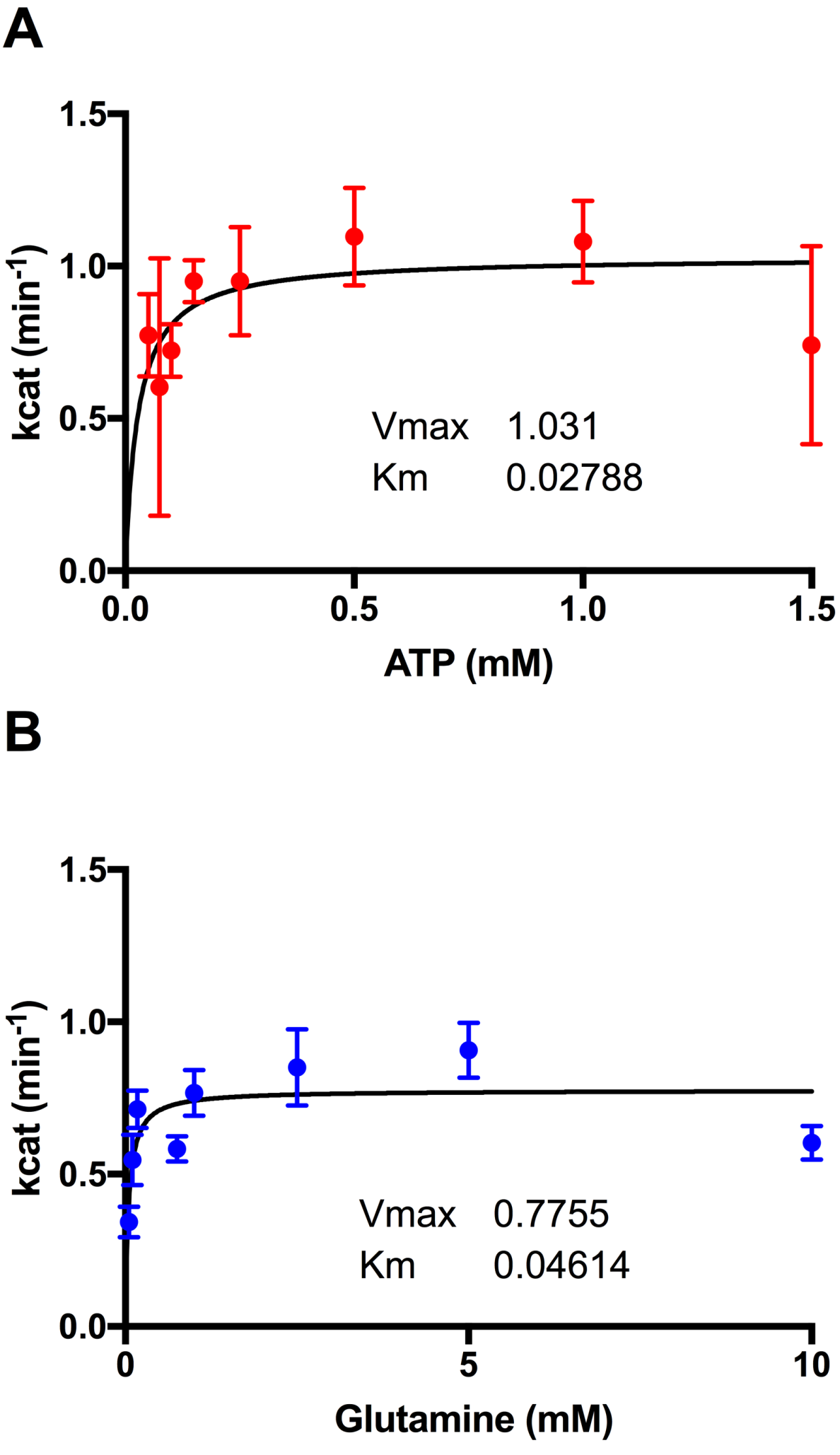
A
1.5
1.0
0.5
0.0
kcat (min-1)
Vmax 1.031
Km 0.02788
0.0
0.5
1.0
1.5
ATP (mM)
B
1.5
1.0
0.5
0.0
kcat (min-1)
Vmax 0.7755
Km 0.04614
0
5
10
Glutamine (mM)

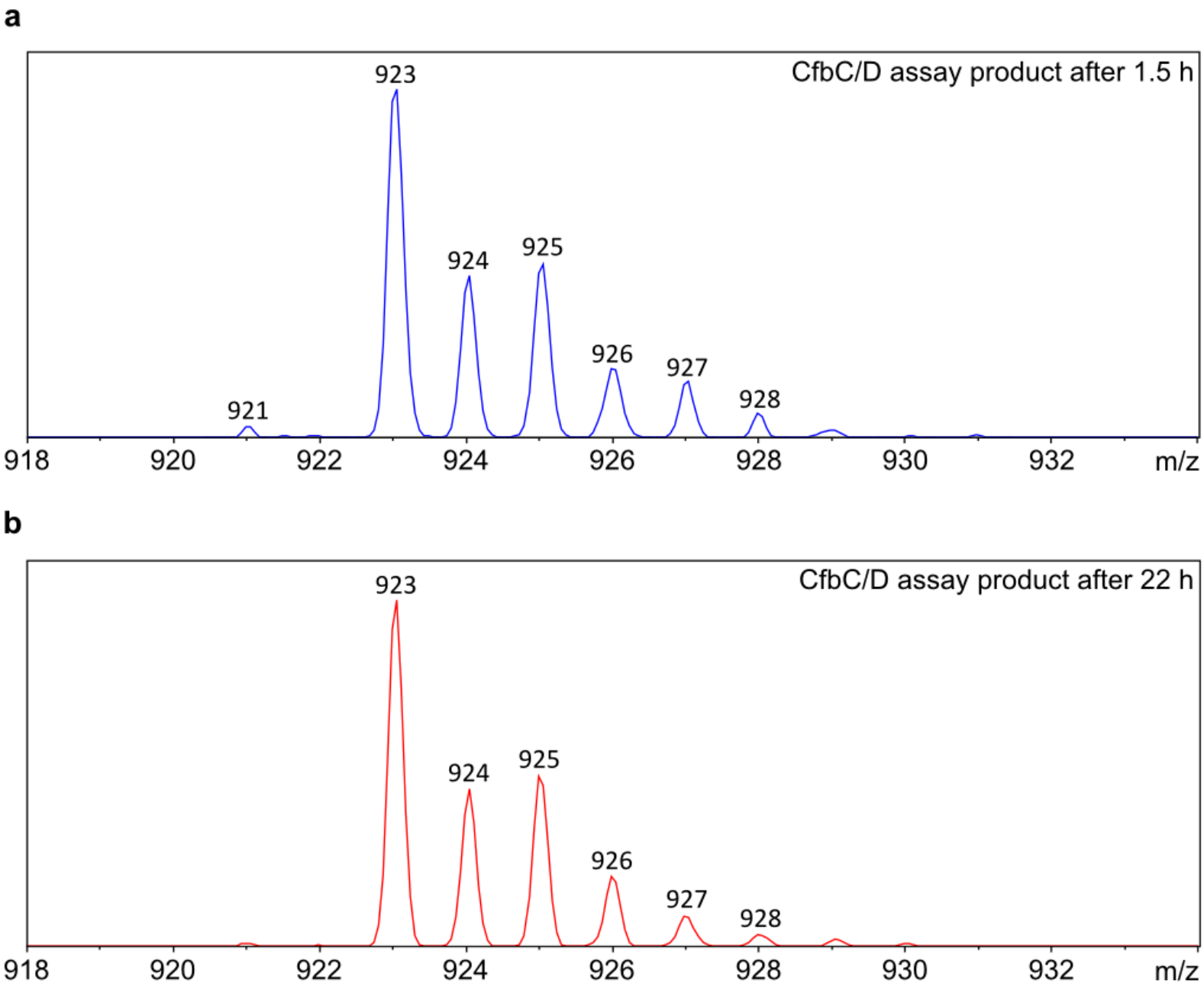
a
CfbC/D assay product after 1.5 h
923
924
925
926
927
928
921
918
920
922
924
926
928
930
932
m/z
b
CfbC/D assay product after 22 h
923
924
925
926
927
928
918
920
922
924
926
928
930
932
m/z

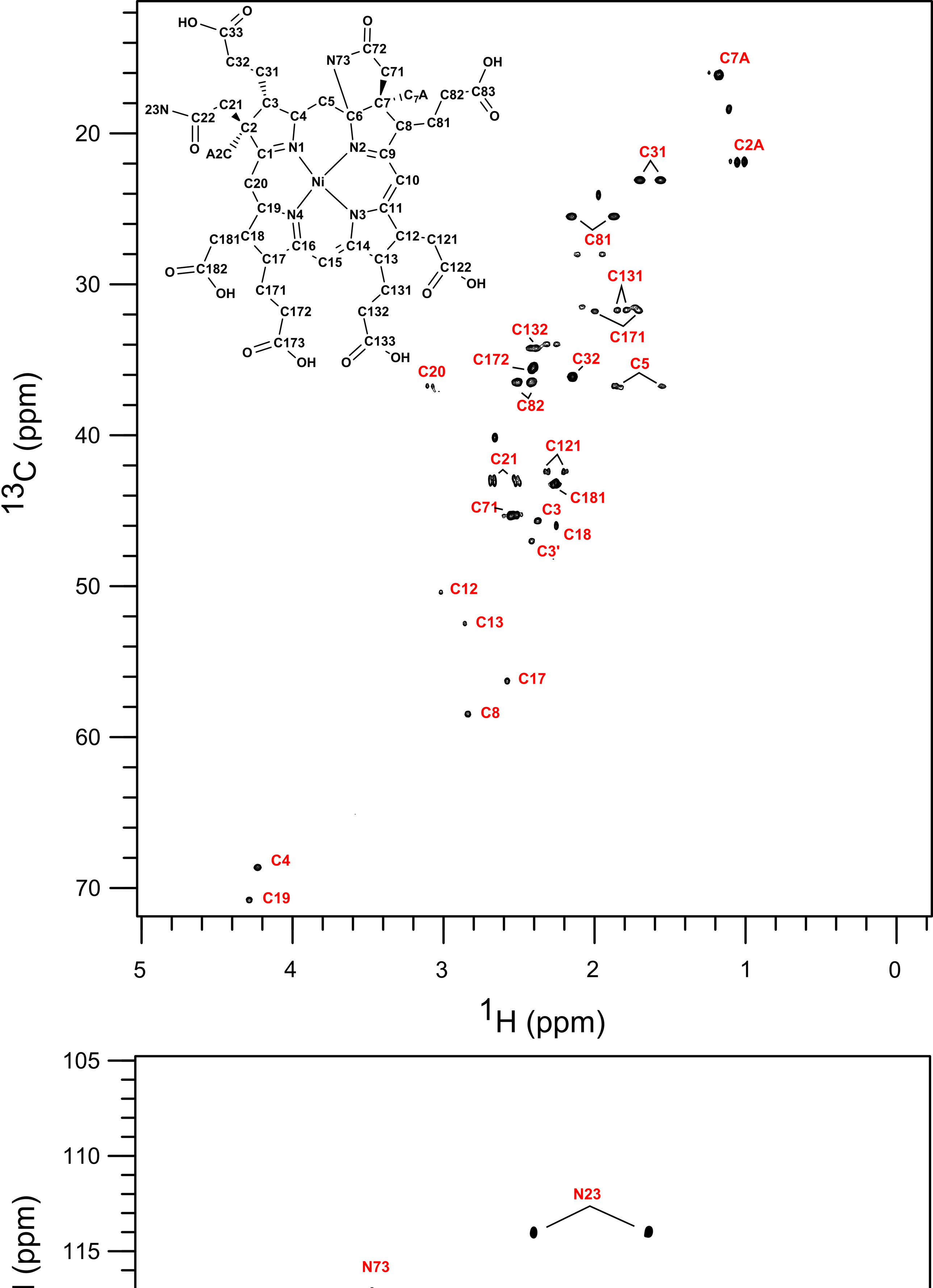
HO
O
C33
C32
C31
23N
C22
O
C21
A2C
C2
C3
C4
C5
N1
C1
N73
O
C72
C71
C6
C7
C7A
C82
C83
OH
O
C8
C81
N2
C9
C10
Ni
C20
C19
N4
N3
C11
C181
C18
C16
C14
C12
C121
C17
C15
C13
O
C182
OH
C171
C131
C122
O
OH
C172
C132
O
C173
OH
C133
O
OH
C20
C7A
C2A
C31
C81
C131
C171
C132
C172
C32
C5
C82
C121
C21
C181
C71
C3
C18
C3'
C12
C13
C17
C8
C4
C19
13C (ppm)
20
30
40
50
60
70
5
4
3
2
1
0
1H (ppm)
105
110
115
120
125
15N (ppm)
N23
N73
10
9
8
7
6
5
1H (ppm)

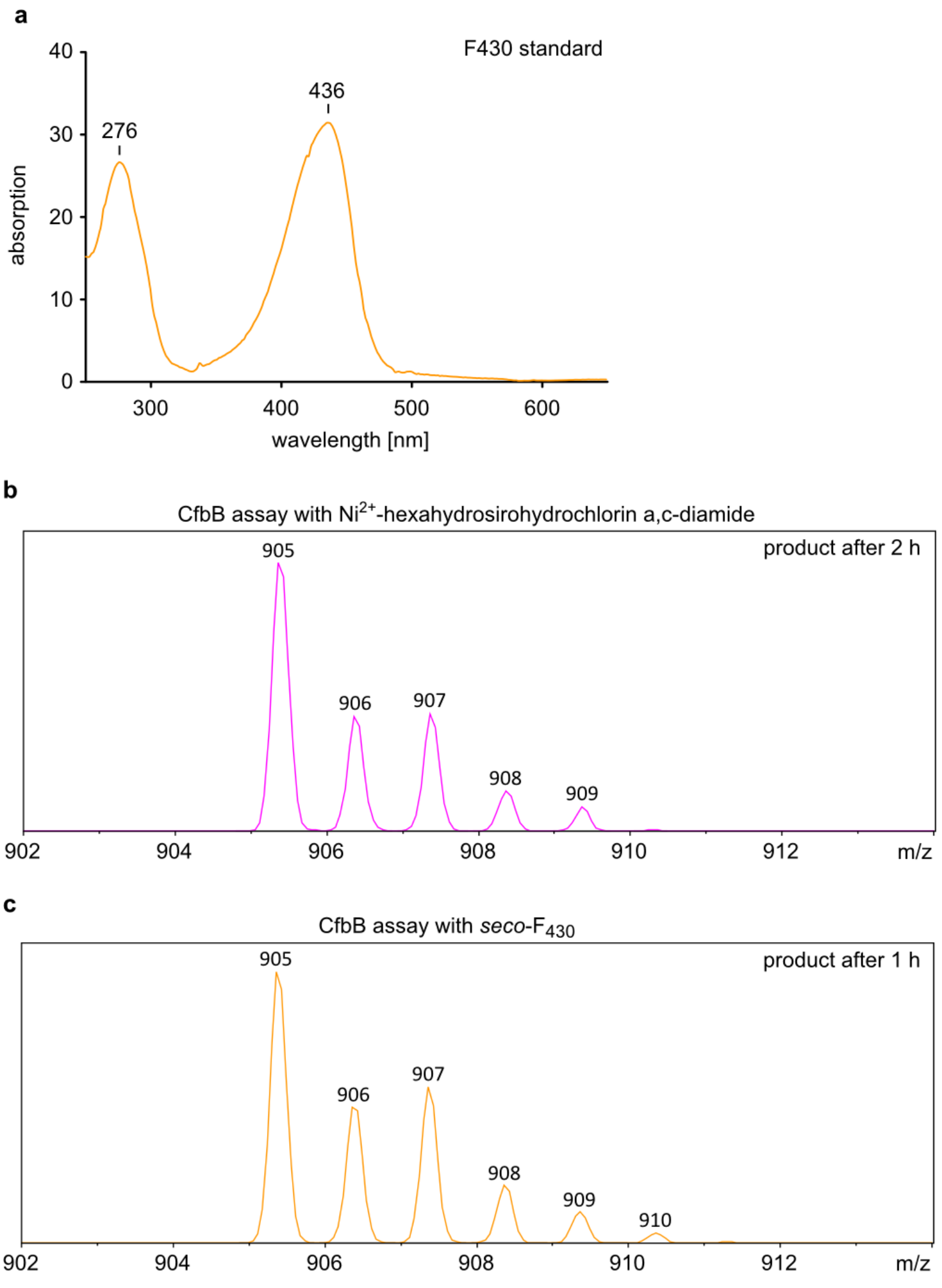
a
F430 standard
436
276
absorption
wavelength [nm]
b
CfbB assay with Ni2+-hexahydrosirohydrochlorin a,c-diamide
product after 2 h
905
906
907
908
909
m/z
c
CfbB assay with seco-F430
product after 1 h
905
906
907
908
909
910
m/z

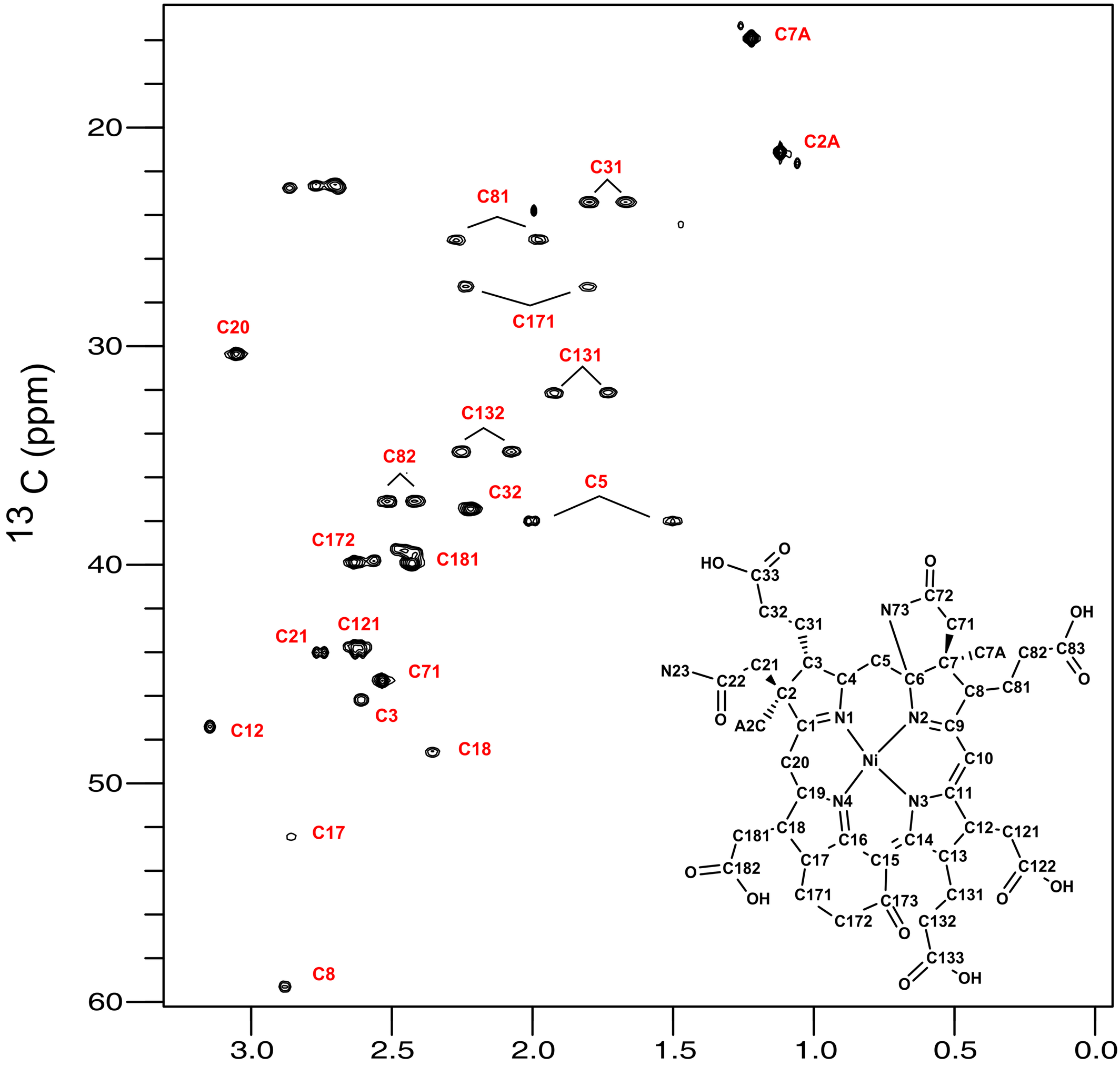
C7A
C2A
C31
C81
C171
C20
C131
C132
C82
C32
C5
C172
C181
C21
C121
C71
C3
C12
C18
C17
C8
20
30
40
50
60
13C (ppm)
3.0
2.5
2.0
1.5
1.0
0.5
0.0
1H (ppm)
HO
C33
O
C32
C31
C72
N73
C71
OH
C83
C82
C81
C7A
C7
C6
C5
C4
C3
C2
C1
N1
N2
C9
C8
C10
C11
N3
N4
C19
C20
Ni
C18
C16
C14
C13
C12
C121
C181
C17
C15
C182
C122
C171
C173
C131
C172
C132
C133
N23
C22
C21
A2C
105
110
115
120
15N (ppm)
9.0
8.5
8.0
7.5
7.0
6.5
6.0
5.5
5.0
1H (ppm)
N23
N73

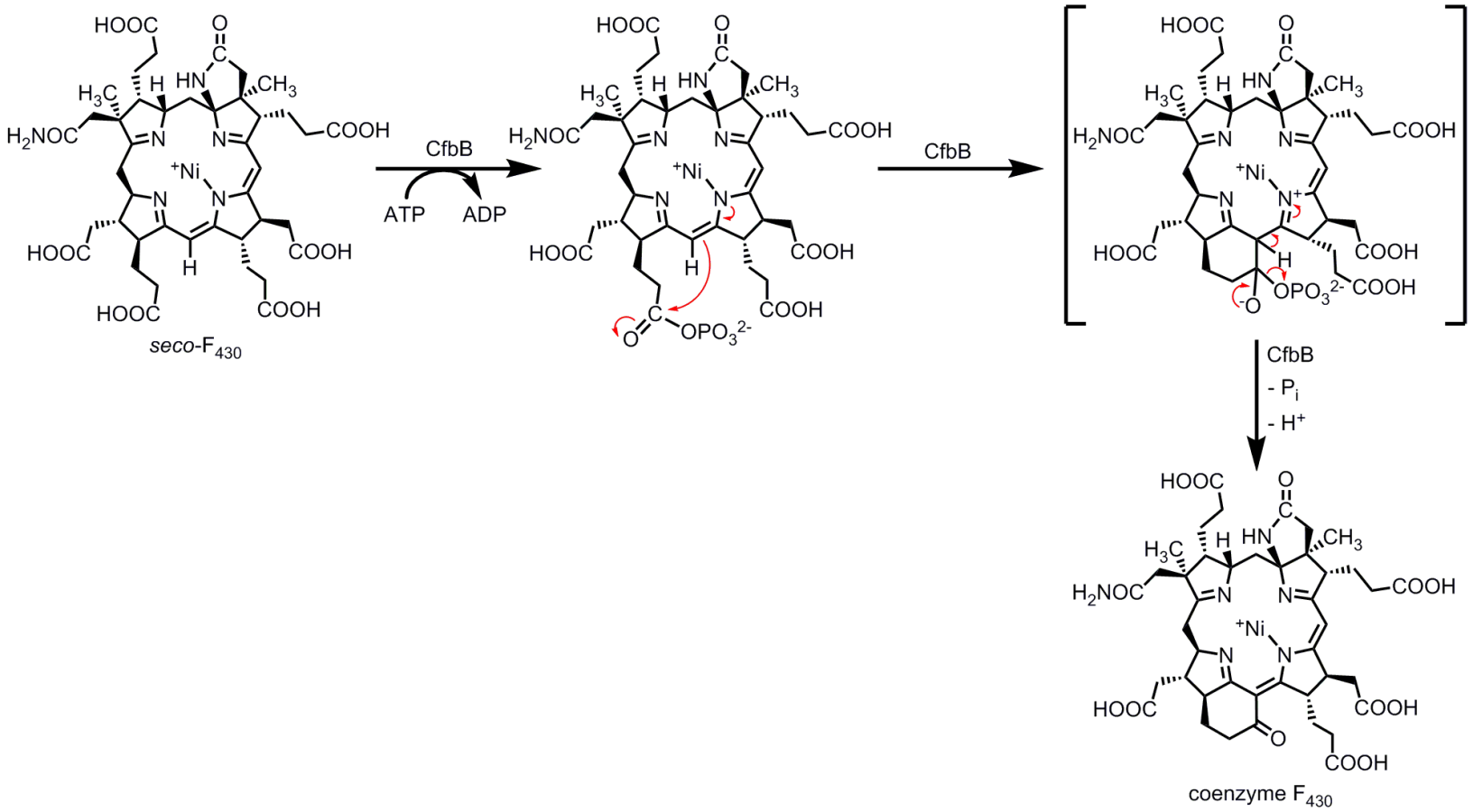
HOOC
O
C
HN
H
H3C
CH3
H2NOC
COOH
N
+Ni
HOOC
H
COOH
HOOC
COOH
seco-F430
CfbB
ATP
ADP
OPO3 2-
CfbB
-O
CfbB
- Pi
- H+
coenzyme F430

Number	Group	$\delta^{1}H$ (ppm)	$\delta^{13}C$ (ppm)
C3	CH	3.68	55.66
C8	CH	3.86	51.19
C2a	CH_2	2.47 2.59	44.95
C3a	CH_2	1.63 2.06	25.03
C3b	CH_2	2.06 2.12	35.22
C7a	CH_2	2.86 3.01	42.62
C8a	CH_2	2.21	24.61
C8b	CH_2	2.4 2.48	36.02
C12a	CH_2	4.02 4.05 4.07 4.09	33.86
C13a	CH_2	3.49 3.54	22.02
C13b	CH_2	2.6	40.17
C17a	CH_2	3.49 3.54	22.02
C17b	CH_2	2.6	40.17
C18a	CH_2	4.02 4.05 4.07 4.09	33.86
C2	CH_3	1.63	19.1
C7	CH_3	1.34	19.53

	δ(1H) [ppm]	δ(13C) [ppm]	δ(15N) [ppm]
C1		190.83	
C2		56.47	
C2A	1.12	21.14	
C21	2.62, 2.76	44.03	
C22		176.18	
N23	6.03, 7.01		108.15
C3	2.61	46.18	
C31	1.67, 1.80	23.41	
C32	2.22	37.45	
C33		182.92	
C4	4.47	67.65	
C5	1.50, 2.00	38	
C6		94.77	
C7		52.06	
C7A	1.22	15.91	
C71	2.53	45.31	
C72		178.38	
N73	7.89		112.19
C8	2.88	59.31	
C81	2.27	25.15	
C82	2.42, 2.52	37.1	
C83		181.75	
C9		179.97	
C10	5.95	100.87	
C11		172.71	
C12	3.15	47.41	
C121	2.63	43.85	
C122		176.22	
C13	3.92	52.37	
C131	1.73, 1.93	32.13	
C132	2.07, 2.25	34.83	
C133		181.62	
C17	2.86	52.44	
C171	1.80, 2.24	27.27	
C172	2.63	39.92	
C173		200.25	
C18	2.36	48.57	
C181	2.43	39.91	
C182		182.32	
C19	3.62	66.05	
C20	3.05	30.36	

	δ(1H) [ppm]	δ(13C) [ppm]	δ(15N) [ppm]
C1		190.9	
C2		56.96	
C2A	1.01	21.89	
C21	2.52, 2.68	43.05	
C22		177.51	
N23	6.75, 7.51		114.02
C3	2.38	45.66	
C31	1.56, 1.70	23.09	
C32	2.15	36.13	
C33		181.82	
C4	4.23	68.64	
C5	1.56, 1.84	36.76	
C6		96.39	
C7		53.19	
C7A	1.17	16.13	
C71	2.54	45.35	
C72		179.85	
N73	8.57		117.18
C8	2.84	58.49	
C81	1.87, 2.16	25.51	
C82	2.43, 2.51	36.48	
C83		181.85	
C9		177.96	
C11		168.05	
C12	3.02	50.41	
C121	2.19, 2.32	42.42	
C122		180.04	
C13	2.86	52.48	
C131	1.79, 1.85	31.7	
C132	2.39, 2.52	34.25	
C133		181.65	
C14		173.17	
C16		172.4	
C17	2.58	56.28	
C171	1.71, 2.00	31.79	
C172	2.4	35.51	
C173		181.92	
C18	2.25	45.99	
C181	2.26	43.21	
C182		180.73	
C19	4.29	70.78	
C20	2.65, 3.09	36.77	